iScience

CellPress
OPEN ACCESS

Article

Class IV Lasso Peptides Synergistically Induce Proliferation of Cancer Cells and Sensitize Them to Doxorubicin

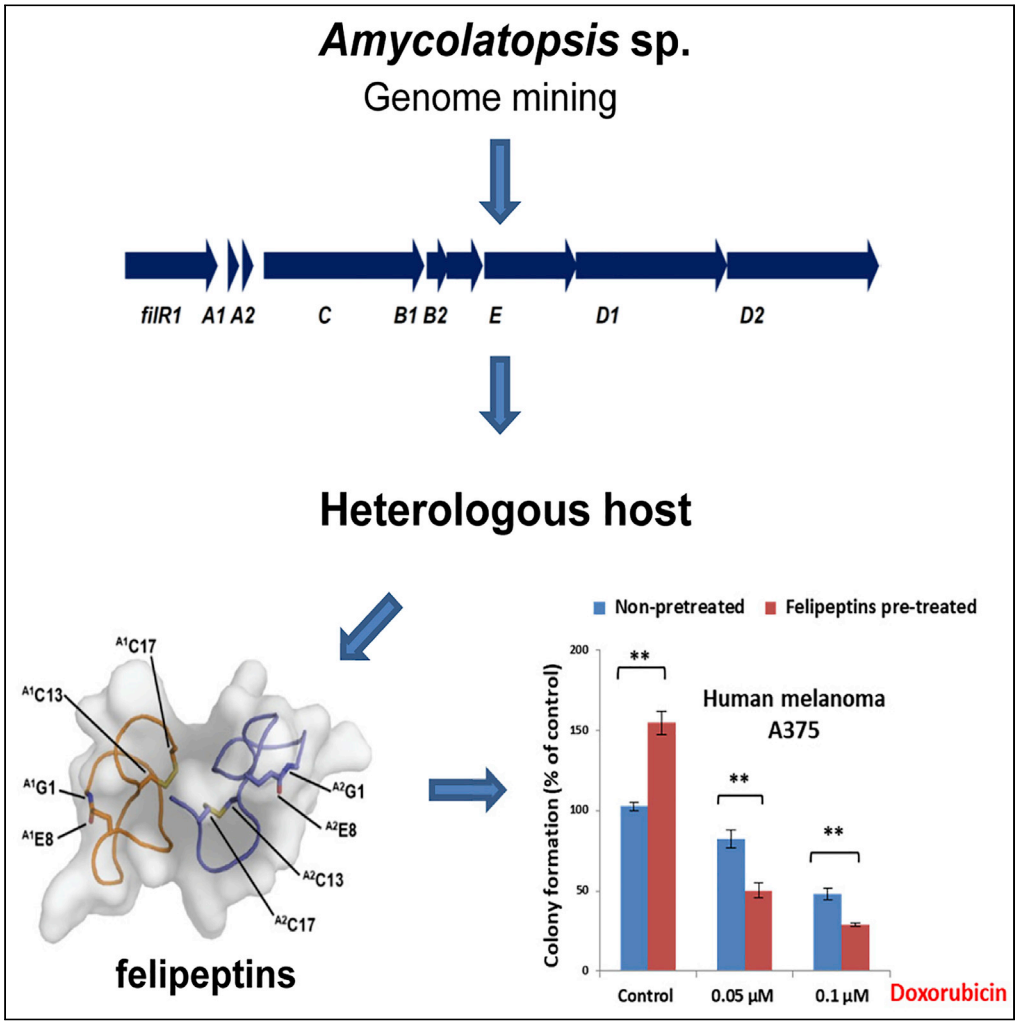

Jaime Felipe Guerrero-Garzón, Eva Madland, Martin Zehl, ..., Cheng-lin Jiang, Galina Selivanova, Sergey B. Zotchev

galina.selivanova@mtc.ki.se (G.S.)
sergey.zotchev@univie.ac.at (S.B.Z.)

HIGHLIGHTS

Lasso peptides felipeptins from *Amycolatopsis* sp. produced in a heterologous host

Felipeptins synergistically sensitize cancer cells to doxorubicin

Synergistic effect on cancer cells appears to be due to complex formation

Felipeptins overcome drug resistance of cancer stem cells

Guerrero-Garzón et al., iScience *23*, 101785 December 18, 2020
https://doi.org/10.1016/j.isci.2020.101785

iScience

CellPress
OPEN ACCESS

Article

Class IV Lasso Peptides Synergistically Induce Proliferation of Cancer Cells and Sensitize Them to Doxorubicin

Jaime Felipe Guerrero-Garzón,[1,9] Eva Madland,[2,9] Martin Zehl,[3] Madhurendra Singh,[4] Shiva Rezaei,[4,5] Finn L. Aachmann,[2] Gaston Courtade,[2] Ernst Urban,[6] Christian Rückert,[7] Tobias Busche,[7] Jörn Kalinowski,[7] Yan-Ru Cao,[8] Yi Jiang,[8] Cheng-lin Jiang,[8] Galina Selivanova,[4,*] and Sergey B. Zotchev[1,10,*]

SUMMARY

Heterologous expression of a biosynthesis gene cluster from *Amycolatopsis* sp. resulted in the discovery of two unique class IV lasso peptides, felipeptins A1 and A2. A mixture of felipeptins stimulated proliferation of cancer cells, while having no such effect on the normal cells. Detailed investigation revealed, that pre-treatment of cancer cells with a mixture of felipeptins resulted in downregulation of the tumor suppressor Rb, making the cancer cells to proliferate faster. Pre-treatment with felipeptins made cancer cells considerably more sensitive to the anticancer agent doxorubicin and re-sensitized doxorubicin-resistant cells to this drug. Structural characterization and binding experiments showed an interaction between felipeptins resulting in complex formation, which explains their synergistic effect. This discovery may open an alternative avenue in cancer treatment, helping to eliminate quiescent cells that often lead to cancer relapse.

INTRODUCTION

Lasso peptides represent a family of ribosomally synthesized and post-translationally modified peptides (RiPPs, Arnison et al., 2013; Maksimov et al., 2012; Hegemann et al., 2013; Tietz et al., 2017), whose biosynthetic gene clusters (BGCs) are present in many bacterial genomes (Hegemann et al., 2013; Mevaere et al., 2018). In recent years, peptide-based bioactive compounds have attracted considerable attention because of their high specificity to molecular targets and because they can relatively easy be re-designed by means of chemical synthesis and/or genetic engineering (Hegemann et al., 2019; de Veer et al., 2019; Pu et al., 2019; Habault and Poyet, 2019). Lasso peptides are small peptides (20 amino acids long, on average) of a unique "lasso" topology with the following features: (i) a macrolactam ring of 7-9 amino acid residues established when the amino group of the N-terminus forms an isopeptide bond with the carboxyl side chain of a glutamic or aspartic acid residue, (ii) the C-terminal tail trapped within the ring either by bulky amino acids or disulfide bridges, or both (Arnison et al., 2013; Hegemann et al., 2013; Li et al., 2015a, 2015b).

Lasso peptides are divided into four classes based on the number and position of disulfide bridges that are important structural features of these RiPPs (Tietz et al., 2017). Class I lasso peptides have two disulfide bridges that link the threaded tail above and below the macrolactam ring. Class II peptides have no disulfide bridges but have a "steric plug" composed of bulky amino acids on either side of the macrolactam ring to help stabilize the fold (Allen et al., 2016; Hegemann et al., 2016; Hegemann, 2020). Class III and IV have only one disulfide bridge. In class III, the disulfide bridge links the tail to the macrolactam ring, whereas in class IV the disulfide bridge is located at the tail itself. So far only two class IV peptides have been characterized, LP2006 from the actinomycete bacterium *Nocardiopsis alba* (PDB accession number 5JPL; Tietz et al., 2017), and pandonodin from *Pandoraea norimbergensis* (PDB accession number 6Q1X; Cheung-Lee et al., 2019).

Bioactivities exhibited by lasso peptides are of definite interest in terms of drug discovery. Some bacterial lasso peptides, such as microcin J25 and capistruin, inhibit RNA polymerase in Gram-negative bacteria and thus have antibiotic activity (Braffman et al., 2019). Others act as antagonists of glucagon receptor (BI-32169; Knappe et al., 2010), endothelin B receptor (RES-701; Morishita et al., 1994) or have inhibitory activity in a cell invasion assay with cancer cells (sungsanpin; Um et al., 2013).

[1]Department of Pharmacognosy, University of Vienna, Vienna 1090, Austria

[2]NOBIPOL, Department of Biotechnology and Food Science, NTNU Norwegian University of Science and Technology, 7034 Trondheim, Norway

[3]Department of Analytical Chemistry, Faculty of Chemistry, University of Vienna, Vienna 1090, Austria

[4]Department of Microbiology, Tumor and Cell Biology, Karolinska Institutet, 17165 Stockholm, Sweden

[5]Department of Animal Biology, Faculty of Natural Sciences, University of Tabriz, Tabriz, Iran

[6]Department of Pharmaceutical Chemistry, University of Vienna, Vienna 1090, Austria

[7]Center for Biotechnology, Bielefeld University, Universitätsstraße 27, 33615 Bielefeld, Germany

[8]Yunnan Institute of Microbiology, Yunnan University, 650091 Kunming, P.R.China

[9]These authors contributed equally

[10]Lead Contact

*Correspondence: galina.selivanova@mtc.ki.se (G.S.), sergey.zotchev@univie.ac.at (S.B.Z.)

https://doi.org/10.1016/j.isci.2020.101785

The minimal set of genes in a lasso peptide BGC encodes a precursor peptide (A) that contains an N-terminal leader and a C-terminal core region sequence, a leader peptide recognition protein (B1), a leader peptidase (B2), and a macrolactam synthase (C). Alternatively, many clusters encode fused B1-B2 proteins. Furthermore, some lasso peptide BGCs can also contain genes for ABC transporters (D), isopeptidases or other additional modification enzymes (Hegemann et al., 2013; Tietz et al., 2017). Significant progress has recently been made in characterization of these proteins, as reported by Yan et al. (2012), DiCaprio et al. (2019), Choudhury et al. (2014), Fage et al. (2016), and Zhu et al. (2016). A study from 2017 provided good insight into the biosynthetic landscape of lasso peptides by identifying BGCs in available bacterial genomes and predicting a total of 1,315 lasso peptide sequences from them (Tietz et al., 2017). This number has nearly doubled in more recent work by de los Santos, who has developed a neural network for identification of RiPP precursor peptides (de los Santos, 2019). Chemical synthesis of lasso peptides is very difficult, and only one example has been reported recently (Chen et al., 2019), suggesting that the best way to produce such peptides and test their biological activities and potential as drug leads is to isolate them after biosynthesis *in vivo*.

The relatively small size of lasso peptide BGCs makes heterologous expression an attractive approach for the production of this class of compounds (Hegemann et al., 2013; Li et al., 2015b; Mevaere et al., 2018; Martin-Gomez et al., 2018). Vast majority of lasso peptides are of proteobacterial origin with only a few examples from actinomycetes. Except for the archetype lasso peptide J25 that was discovered in its native host, *Escherichia coli*, proteobacterial lasso peptides have typically been produced via heterologous expression. Sviceucin is the only lasso peptide from an actinomycete bacterium that has been produced via heterologous expression in considerably high quantities (Li et al., 2015a). Therefore, further attempts on expression of lasso peptide BGCs must be pursued in order to gain access to the diversity of lasso peptides, especially from actinomycete bacteria. This is particularly relevant for class IV lasso peptides, which are rare and poorly biologically characterized so far.

In this work, we present the successful genome mining of a newly isolated *Amycolatopsis* sp., leading to the heterologous expression, purification, structural and biological characterization of two class IV lasso peptides exhibiting unique synergistic biological activity, which may prove useful in combinational cancer chemotherapy.

RESULTS AND DISCUSSION

Amycolatopsis sp. YIM10 Metabolites and Genome Analyses

Amycolatopsis sp. YIM10 was isolated from a rare earth mine of Bayan Obo, Inner Mongolia, China, and taxonomically identified by means of 16S rRNA gene sequencing. Cultivation of this isolate in different conditions revealed its ability to produce various tiglosides and 1,2,4-trimethoxynaphthalene, as suggested by Liquid Chromatography-Mass Spectrometry (LC-MS) analyses (Figures S1–S4, Supplemental Information). While these natural products have been described previously (Guo et al., 2012; Rycroft et al., 1998), the latter has never been isolated from a bacterium before. The structures of these compounds were also confirmed using Nuclear Magnetic Resonance (NMR) spectroscopy (Figures S5 and S6, Supplemental Information). No compounds with strong antimicrobial activity could be identified in these initial experiments. Keeping in mind the reported potential of *Amycolatopsis* spp. to produce bioactive secondary metabolites, the genome of YIM10 was completely sequenced (GenBank: CP045480, Table S3) and found to consist of a circular chromosome of 10.31 Mb and a 39.9 Kb plasmid. The genome was analyzed with antiSMASH 5.0 software (Blin et al., 2019), which identified at least 44 secondary metabolite BGCs. Several of these BGCs appear to be unique and could not be identified in the publicly available genomes of other bacteria (Table S4, Supplemental Information). The vast majority of BGCs identified in the genome of YIM10 had homologs in the genome of recently described *Amycolatopsis albispora* WP1 isolated from marine sediment (Wu et al., 2018), suggesting that these strains are closely related.

Given that the genome of *Amycolatopsis* sp. YIM10 contains uncharacterized BGCs and therefore may have a potential to produce previously undescribed compounds, it was regarded as an excellent candidate for genome mining. First, this strain was evaluated as a possible subject for genetic manipulation. However, YIM10 was found to be resistant to all the antibiotics used as selection markers in actinomycetes, in particular apramycin, hygromycin, thiostrepton, kanamycin, and puromycin. Thus, establishing a gene transfer system for this bacterium appeared problematic. Considering this, cloning and expression of BGCs in a heterologous host seemed like the only strategy to circumvent the problem. Therefore, a YIM10 fosmid

Gene	Gene product
filR1	transcriptional regulator (SARP family)
filA1	felipeptin A1 lasso peptide precursor
filA2	felipeptin A2 lasso peptide precursor
filC	asparagine synthase (lasso cyclase)
filB1	PqqD family protein (leader peptide binding)
filB2	transglutaminase-like superfamily protein (leader peptidase)
filE	LLM class flavin-dependent oxidoreductase (disulfide bridge formation)
filD1	ABC transporter (lasso peptide efflux)
filD2	ABC transporter (lasso peptide efflux)

Figure 1. Lasso Peptide Biosynthesis Gene Cluster from *Amycolatopsis* sp. YIM10: Organization of Genes and Predicted Functions of Their Products

genome library was constructed (Supplemental Information, Transparent Methods). We were particularly interested in expressing BGC21, which was predicted to govern biosynthesis of two class IV lasso peptides (MiBIG accession number BGC0002064). This BGC spans ~10 kb and contains all the main genes for the biosynthesis of this class of RiPPs.

Screening of the genome library using pooled PCR with primers designed for flanking and central regions of BGC21 led to the identification of a single fosmid containing the entire cluster. BGC21 (Figure 1) harbors two genes encoding precursor peptides (*filA1* and *filA2*), as well as genes for the proteins involved in the leader peptide recognition and cleavage (*filB1* and *filB2*), the macrolactam ring formation (*filC*), putative oxidoreductase-catalyzed reactions (*filE*), transport (*filD1* and *filD2*), and transcriptional regulation (*filR1*).

A cassette containing an *oriT* sequence and integration site int-attPϕC31 allowing conjugative transfer of the construct into *Streptomyces* bacteria and stable genomic integration, respectively, was incorporated into the identified fosmid using λ RED recombineering (Supplemental Information, Transparent Methods). The recombinant fosmid harboring BGC21 was introduced into *Streptomyces coelicolor* M1154 engineered for heterologous expression of exogenous BGCs (Gomez-Escribano and Bibb, 2011) and *Streptomyces albus* J1074. The resulting recombinant strains were cultivated in different liquid and solid media, but no lasso peptide production could be detected in these conditions.

Next, the gene *filR1* encoding a transcriptional regulator of the SARP family, was cloned into the plasmid pSOK806 under control of the strong constitutive promoter ermEp* (Mevaere et al., 2018). The construct was conjugated into the abovementioned *Streptomyces* hosts that harbored integrated recombinant fosmid with BGC21. The constitutive overexpression of the FilR1 SARP regulator apparently triggered the production of both predicted lasso peptides in the two *Streptomyces* hosts when cultivated in liquid MYM medium (Figures S7 and S8, Supplemental Information). The detected lasso peptides were designated felipeptins A1 and A2, and predicted, based on the sequence data, to be composed of 18 and 17 amino acids, respectively.

Given that the *S. coelicolor* M1154 host has a cleaner metabolic background compared to that of *S. albus* J1074, and virtually no differences in lasso peptides yields were found between the two strains (data not shown), it was decided to work further only with the former recombinant strain.

Structure Elucidation by LC-MS and NMR Confirms the Identity of Two Class IV Lasso Peptides

Up-scaled fermentation and optimization of the purification protocol resulted in production yields of 12 mg/L of felipeptin A1, and 7 mg/L of felipeptin A2 (see Transparent Methods). These yields are significantly higher than those usually obtained after heterologous expression of lasso peptides BGCs (Li et al., 2015a; Mevaere et al., 2018; Martin-Gomez et al., 2018). Most likely, this is due to overexpression of the SARP regulator encoded by the felipeptins BGCs, which apparently controls expression of all other biosynthetic genes in the cluster. The measured molecular masses of felipeptin A1 (HRESIMS *m/z* 1009.4640 $[M+2H]^{2+}$; calculated for $C_{91}H_{130}N_{26}O_{23}S_2^{2+}$, *m/z* 1009.4616, Δ = 2.4 ppm) and felipeptin A2 (HRESIMS

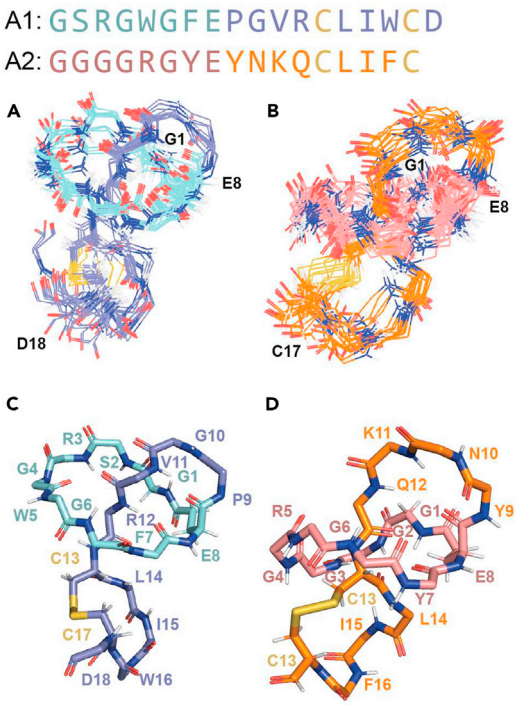

Figure 2. Structures of Felipeptins A1 and A2

(A and B) NMR ensemble structures of (A) felipeptin A1 PDB:6TXH and (B) A2 PDB:6TXI. The structures depict the looped-handcuff topology stabilized by a disulfide bridge, characteristic of class IV lasso peptides. In both structures, amino acids G1-E8 in the macrolactam ring are colored lighter, and the disulfide bridges, C13-C17, are colored yellow.

(C and D) The amino acid sequences and lowest energy conformers for felipeptins A1 (C) and A2 (D) are also shown.

m/z 922.9145 $[M+2H]^{2+}$; calculated for $C_{81}H_{119}N_{23}O_{23}S_2^{2+}$, *m/z* 922.9140, Δ = 0.5 ppm) matched well with the peptide sequences GSRGWGFEPGVRCLIWCD and GGGGRGYEYNKQCLIFC predicted from the *filA1* and *filA1* gene products, respectively, provided that two macrocycles are formed (Figure S8, Supplemental Information). The purity of felipeptins was verified using High Performance Liquid Chromatography (HPLC) and LC-MS (Figures S9 and S10, Supplemental Information).

The structures of both felipeptins (Figure 2) were elucidated using an NMR-based approach, with dimethylsulfoxide (DMSO) as the solvent (see Transparent Methods). The structures depict an 18-mer peptide (felipeptin A1) and 17-mer peptide (felipeptin A2) with a looped-handcuff topology. Both peptides have an eight amino acid macrolactam ring at the N-terminus formed by condensation of the side chain of Glu8 and the free N-terminus of Gly1. The formation of the isopeptide bond is confirmed by the long-range nuclear Overhauser effect (NOE) peak between these two residues. For both felipeptins, threading of the loop region through the macrolactam ring is confirmed by the long-range NOEs (H^{α} Trp5–H^{α} Arg12 and H^{N} Gly6–H^{α} Arg12). Formation of a disulfide bridge (Cys13-Cys17) in both felipeptins was confirmed by long-range NOEs between H^{α} of Cys17 and H^{β} of Cys13. This disulfide bond might serve as a stabilizing feature by "trapping" the tail in position. Other structural features that might serve as steric locks are Val11 (in A1) and Gln12 (in A2) above the macrolactam ring, as well as Arg12 and Leu14 (in A1) and Leu14 (in A2) below the ring. The A1 and A2 structures have been deposited in the Protein Data Bank under the accession IDs 6XTH and 6XTI, respectively.

Structural features were also confirmed by the spectra of the two lasso peptides, obtained after tandem MS (Rosengren et al., 2004; Jeanne Dit Fouque et al., 2019),which showed a series of abundant a-, b-, and y-type peptide fragment ions covering the linear chain encompassing amino acids 9–12. Their masses fit to the expected macrolactam ring formation between the N-terminal Gly formed after removal of leader peptides and the side chain of Glu8 on one side, as well as the formation of a second macrocycle via a disulfide bridge between Cys-residues in positions 13 and 17 (Figure 3).

The Proposed Biosynthesis of the Felipeptins A1 and A2 Requires FilB1, FilB2, FilC, and FilE for Mature Lasso Peptide Formation

Based on the current knowledge on the functions of the lasso peptide biosynthesis enzymes, and the presence of a gene *filE* encoding an oxidoreductase, the biosynthesis of felipeptins was predicted as shown in Figure 4.

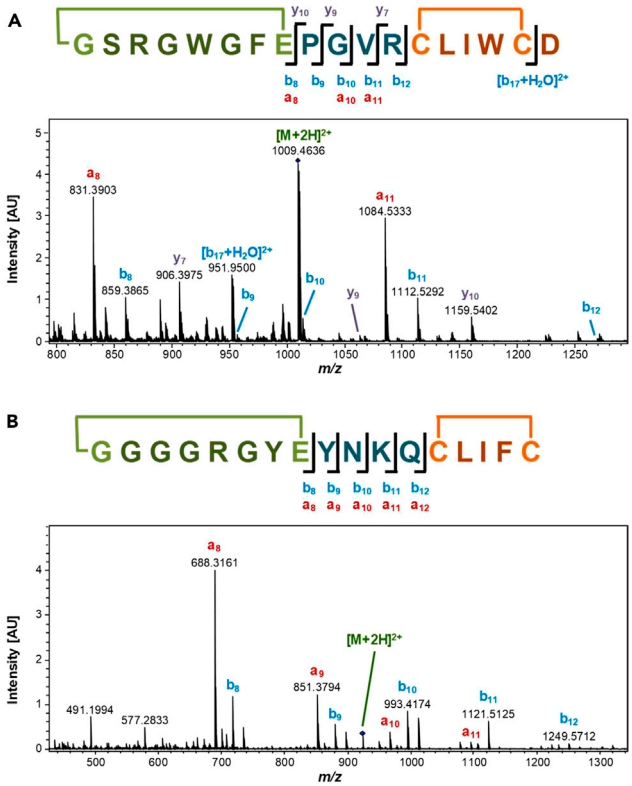

Figure 3. MS Spectra of Felipeptins A1 and A2 Showing Formation of Two Macrocycles

(A and B) HRESIMS/MS spectra of the [M+2H]2 + ions of felipeptin A1 at m/z 1009.4640 (A) and felipeptin A2 at m/z 922.9145 (B). The fragmentation, occurring mainly in the linear region between the two macrocycles, fully confirms the structures predicted from the BGC data.

According to the proposed biosynthetic pathway, the FilB1 protein recognizes the precursor peptides, products of *filA1* and *filA2* genes, and guides them to the peptidase FilB2, which cleaves off leader peptides (DiCaprio et al., 2019; Koos and Link, 2019). Immediately after cleavage, the lasso cyclase FilC forms a macrolactam ring and assists in the lasso-fold formation. The last step in the biosynthesis is most likely accomplished by an oxidoreductase FilE, which forms disulfide bridges, stabilizing the final structures. Interestingly, database searches for proteins similar to FilE revealed only those with less than 55% identity, suggesting this oxidoreductase being rather unique.

Since the only other member of class IV lasso peptides biologically characterized, LP2006, displayed antibacterial activity, we tested felipeptins A1 and A2 against a panel of different Gram-positive bacteria in liquid media-based assays in order to determine minimal inhibitory concentrations. The results obtained suggest that felipeptins and their combination do not exhibit antibiotic properties, except in the cases of *Streptococcus pyogenes* and *Streptococcus pneumoniae*, where felipeptin A1 and the 1:1 A1+A2 mixture showed weak antibacterial activity (Table S5, Supplemental Information). Interestingly, in the case of *S. pyogenes*, only a mixture of felipeptins was found to be active. The synergistic effect was also clearly visible with the disk diffusion assay performed using *Bacillus subtilis* as test organism (Figure S11, Supplemental Information).

Felipeptins A1 and A2 Exert a Unique Synergistic Effect on Cancer Cells

In order to evaluate other possible bioactivities of felipeptins A1 and A2, we tested the effect of a range of concentrations of felipeptins and their combination in cell viability assays using several cancer cell lines of different origin, including colon carcinoma HCT116, melanoma A375, and breast carcinoma MCF7, in comparison to normal cells, the human fibroblast cell line BJ and bone marrow-derived mesenchymal stem cells (MSCs). While individual peptide treatments had marginal and statistically insignificant effects on the

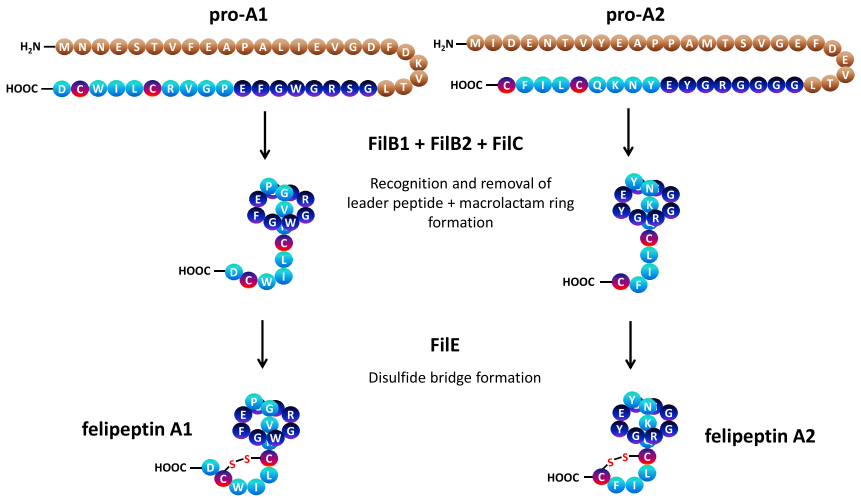

Figure 4. Proposed Felipeptins Biosynthesis Pathway

number of viable MCF7, HCT116, and A375 cells, their combination at certain ratios significantly increased the number of viable cancer cells in three cell lines (Figures 5A–5C, left panels and Figures S12A and S12B). The effect of felipeptins combinations at several doses was synergistic, as shown in Figures 5A–5C (green squares). In contrast, the effect of felipeptins on the growth rate of normal cells, BJ and MSC, was weak and without synergistic effect (Figures 5D and S12C).

Since the increased number of cells could be due to either lower rate of cell death or higher rate of cell proliferation, we investigated the effect of felipeptins on cell cycle distribution using fluorescence-assisted cell sorting (FACS) of propidium iodide–stained cells (Figures 6A–6C). While no change in the fraction of dead cells (subG1 fraction, <2N DNA content) could be observed, a decrease of cells in G1 (cell cycle preparatory phase, 2N DNA content) concomitantly with the increase of cells with >2N DNA content, i.e., cells in replication (S) and cell division (G2/M) phases was evident. These data clearly indicated an enhanced rate of proliferation.

To better understand the mechanism of pro-proliferative activity of felipeptins, we tested the involvement of tumor suppressors p53 and Rb, the two key factors that control the decisions of cells to proliferate (Hanahan and Weinberg, 2011). We addressed the involvement of p53 by using two cancer cell lines, MCF7p53KO and A375p53KO, in which the p53 gene was deleted by means of CRISPR-Cas9-mediated gene editing. However, the deletion of p53 did not significantly affect the pro-proliferative activity of felipeptins and their combinations (Figures S12D and S12E, Supplemental Information). Importantly, the observed statistically significant changes in the proportion of cells in different phases of the cell cycle, although minor, were qualitatively and quantitatively similar to those exhibited upon deletion of the gene for the retinoblastoma protein Rb (Brugarolas et al., 1998). In addition, we found a significant decrease in the level of the Rb protein and phosphorylated Rb upon felipeptin treatment in A375 cells, as assessed by immunoblotting (Figure 6D). Taken together, our data suggest that the inhibition of Rb is involved in stimulation of proliferation by felipeptins.

The concept that quiescent cancer stem-like cells (CSCs) within solid and hematological cancers confer resistance to chemo- and irradiation therapy, which preferentially targets rapidly proliferating cells, is currently widely accepted (Hanahan and Weinberg, 2011; Brown et al., 2017). Based on our data on stimulation of the cancer cell proliferation by felipeptins, we addressed the question of whether pre-treatment with felipeptins can increase the cytotoxic activity of the widely used chemotherapeutic drug doxorubicin (DOX). Importantly, we found that pre-treatment of MCF7 and A375 cells with felipeptins significantly and synergistically increased the efficiency of cancer cell suppression by doxorubicin (Figures 7A and 7B, left panels). The quantification of the synergistic effect of combination ratios is presented in the left panels In Figures 7A and 7B (green squares). Further confirmation of the potentially beneficial effect of pre-treatment with felipeptins was obtained in a long-term (7 days) colony formation assay. In this experiment, the

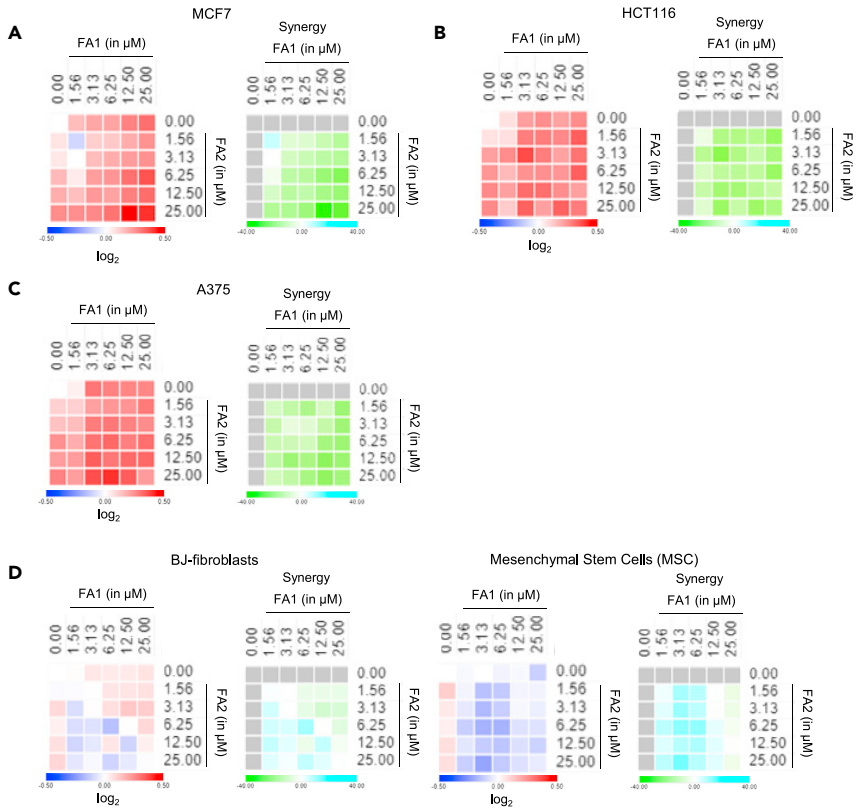

Figure 5. Synergistic Induction of Cancer Cell Proliferation by Felipeptins

(A–D) Left panels, heatmaps show changes of the number of viable cells upon 72 hr treatment with different doses of felipeptins and their combinations at a 2-fold serial dilution (as indicated in the figures) in cancer cell lines MCF7 (A), A375 (B), HCT116 (C) and normal cells, BJ fibroblasts and bone marrow-derived mesenchymal stem cells MSC (D), measured using resazurin assay and normalized to DMSO control. Red indicates increased cell number, white – no change, blue – decreased cell number. Right panels, heatmaps show Highest Single Agent (HSA) reference model score, indicated by green color (A-D). Data are presented as mean log2 from two independent experiments performed in duplicate.

A375 cells were pre-treated with a combination of 6.25 μM and 12.5 μM of felipeptins for 72hr, followed by 72hr DOX treatment. The number of cancer cell colonies was decreased much more efficiently by DOX upon pre-treatment with felipeptins (Figure 7C), demonstrating a remarkable increase in sensitivity toward DOX in comparison with the non-pretreated cells. Furthermore, the number of cells in the colonies was considerably lower in the felipeptins pre-treated samples. A number of studies have found that DOX has high propensity to select for drug-resistant cancer stem cells in previously differentiated cancer cells of various human solid tumors, including lung and breast carcinoma, neuroblastoma and osteosarcoma (Martins-Neves et al., 2018). Calcagno et al. have demonstrated that prolonged exposure of the MCF-7 breast cancer cells to doxorubicin selects for cells with a drug-resistant phenotype, enriched in stem cells with increased invasiveness and tumorigenicity (Calcagno et al., 2010).

Following the previously described protocol (Calcagno et al., 2010), we selected DOX-resistant MCF7 cells and tested whether stimulation of their growth by felipeptins will overcome resistance to DOX (Figure 7D). As shown in Figure 7E, cells pre-treated with felipeptines were much more sensitive to the second treatment with DOX. Felipeptins decreased the number of drug-resistant colonies almost 4-fold. Moreover, as can be seen in Figure 7F, the remaining colonies contained fewer cancer cells, while the phenotype of some of those remaining cells (big, flat cells) suggests that they entered irreversible growth arrest (senescence), preventing their recurrent growth. Thus, our data demonstrate that stimulating the proliferation of drug-resistant cancer stem cells by felipeptins re-sensitized them to chemotherapy and overcame drug resistance.

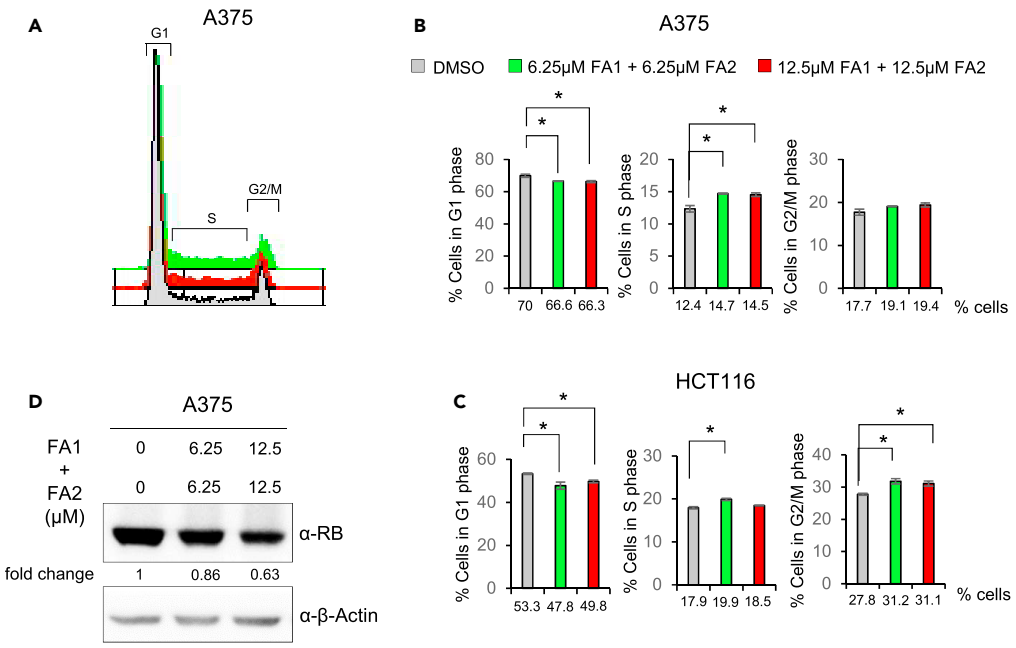

Figure 6. Felipeptins Stimulate Proliferation of Cancer Cells via Inhibition of pRb

(A and C) Stimulation of cell cycle progression by 24hr treatment with felipeptins (green bars, 6.25 μM each; red bars, 12.5 μM each) as detected by FACS of propidium iodide–stained A375 (A, B) and HCT116 (C) cell lines. Gray bars, control DMSO treatment. Data are shown as mean ± SD from two independent experiments. *$p < 0.05$, unpaired t test.

(D) Western blotting for total RB and phospho-Rb in A375 upon felipeptins treatment for 24 hr β-Actin is used as a loading control.

Notably, the biological effect of combined felipeptins was dependent on the cell type. The selective effect of felipeptins on different types of cells lead us to speculate that the combination of felipeptins A1 and A2 might mimic a growth factor, hormone or cytokine, which are known to have differential effects on different types of cells. For example, activin A, which belongs to the transforming growth factor β superfamily, can exert both proliferative and anti-proliferative effects depending on the differentiation stage of the cell and the presence of other growth factors in the system (Bloise et al., 2019). Further high throughput studies are required to dissect the exact mechanism of the selective biological activity of felipeptins.

Synergistic Biological Effect of Felipeptins Is Likely due to Complex Formation

In order to further investigate the synergistic effect between felipeptins A1 and A2, we performed an NMR titration experiment to measure the strength of the interaction (dissociation constant; K_d) between them (Supplemental Information). ^{13}C-HSQC spectra of felipeptin A2 were recorded before and after addition of felipeptin A1. Upon increasing the concentration of felipeptin A1, we observed a chemical shift perturbation in certain residues (side-chains of Arg5, Tyr7, Lys11, and Ile15; backbone of Lys11) in felipeptin A2. These affected residues were confirmed by chemical shift perturbations observed in an ^{15}N-HSQC spectrum recorded at the end of the titration (Supplemental Information, Figure S12). These chemical shift perturbations indicate a change in the chemical environment of the observed ^{1}H-^{13}C atom pairs that were used to estimate a $K_d = 0.3 \pm 0.2$ mM for the interaction (Figure S12). The amino acid–specific locations of the highest chemical shift perturbations were used to guide the docking of felipeptins A1 and A2 using HADDOCK (van Zundert et al., 2016).

Figure S12 (Supplemental Information) shows a HADDOCK model, where the ring of one felipeptin interacts with the tail of the other (see figure text of Figure S12 for further discussion). While the NMR data fits best with a model in which felipeptins interact in a 1:1 ratio, we cannot rule out the possibility of a model where felipeptins interact in other ratios. NMR studies were performed in DMSO due to the poor solubility of the felipeptins in water (see Transparent Methods). While the observation of the interaction between felipeptins under these conditions does not entail the existence of an interaction under physiological conditions, it does not rule it out either.

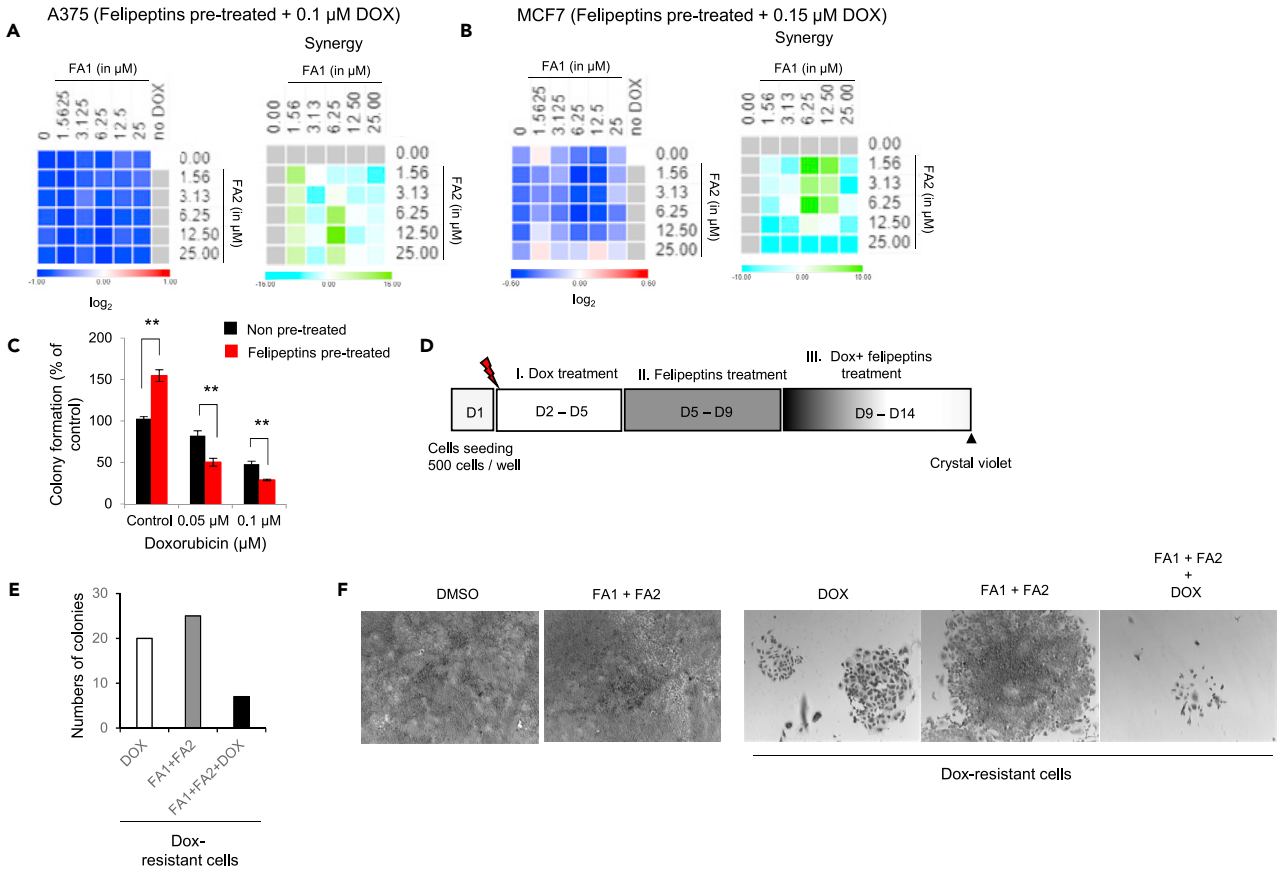

Figure 7. Felipeptins Sensitize Cancer Cells to Doxorubicin and Overcome Drug Resistance of Cancer Stem Cells

(A and B) Heatmaps (left panels) reflect the number of viable cells in A375 (A) and MCF7 (B) cell lines, pre-treated with different concentrations of felipeptins for 72hr followed by doxorubicin for another 72hr. HAS Synergy scores (right panels) are indicated in green color. Data are presented as mean log2 from two independent experiments performed in duplicate.

(C) Long-term viability assay (7-day colony formation) in A375 cells, pre-treated or not pre-treated with felipeptins A1+A2 before applying doxorubicin as in (A). Colonies were detected using crystal violet staining. The charts illustrate the percentage of the colony numbers relative to the untreated control. ** $0.01 \leq p$.

(D). Schematic illustration of the experiment. I – Doxorubicin-resistant MCF-7 cancer stem cells were obtained upon 72hr treatment by 12.5 nM doxorubicin. II – Their growth was stimulated by combination of felipeptins (25 μM each) for 96 hr. III – Resulting colonies were treated by the same doses of DOX or felipeptins or Dox/felipeptins combination for 5 days.

(E) Quantification of drug-resistant colonies obtained as in (D) upon treatment of DOX or felipeptins or their combination. Colonies were detected using crystal violet staining; colonies were counted using ImageJ analysis.

(F) Representative phase-contrast microscopy image of crystal violet-stained colonies obtained as shown in (D).

Whatever the molecular mechanism behind the specific stimulation of cancer cell proliferation by felipeptins is, this unique biological activity may open interesting possibilities for combinational cancer therapy. Accumulated experimental evidence increasingly supports the notion that the persistence of quiescent subpopulations of cancer cells, including CSCs, cause relapse after initially successful chemotherapeutic treatment (Battle and Clevers, 2017). However, targeting quiescent CSCs remains a major challenge. A possible strategy could be to 'wake up' this cell population to increase its susceptibility to chemotherapy, as it has been demonstrated by genetic means in experimental models of chronic myeloid leukemia (Takeishi et al., 2013).

Thermal and Proteolytic Stability of Felipeptins

Considering presumed potential of felipeptins in being used in therapy, it appeared necessary to test their thermal and proteolytic stability. To assess the thermal stability of the felipeptins and the stabilizing role of the disulfide bond, aqueous solutions were incubated at 95°C for 20hr in the absence and presence of the

reducing agent dithiothreitol (DTT) (Allen et al., 2016; Zong et al., 2017; Hegemann, 2020). Felipeptin A1 showed no sign of thermal unthreading after 20hr at 95°C, even though partial hydrolytic cleavage of the C-terminal Asp18 was already observed. In the presence of DTT, not only reduction of the disulfide bond but also further chemical cleavage was detected, proving the stabilizing role of the disulfide bond (Figure S14).

Felipeptin A2 also showed remarkable thermal stability, but the appearance of an additional peak in the chromatogram strongly indicated partial thermal unthreading after 20hr at 95°C (Figure S15). The MS data for this additional peak proof identical mass and the MS/MS spectrum shows identical fragment ions that were, however, detected with altered relative intensities, indicating a different peptide fold (Figure S16). Both peptides were stable toward carboxypeptides B and Y, which might as well be attributed to the lasso-fold (Figures S17 and S18), as well as to the disulfide bond close the C-terminus. Considering the size of the macrocycle formed by the disulfide bond (Figure 2), it can be assumed that thermal unthreading proceeds via the tail pulling mechanism only but which structural features determine the even higher stability of felipeptin A1 compared to A2 requires further detailed studies (Hegemann, 2020).

The high thermal and proteolytic stability observed for the felipeptins is definitely a big advantage when considering up-scaled biotechnological production and potential medical applications. Most of the current chemotherapeutic agents used for cancer treatment are designed to target rapidly dividing cancer cells, which are thus becoming more vulnerable to cytotoxic agents compared to normal cells. However, in many cases seemingly successful treatments of cancers still end up in relapse, owing to the dormant cancer cells that survive the treatment in a quiescent state. Pre-treatment of cancer cells with felipeptins sensitizes them to doxorubicin, a widely used chemotherapeutic agent, and may provide an opportunity to reduce the dosage of this cytotoxic agent and thereby minimize side effects. Moreover, pre-treatment of doxorubicin-resistant cancer cells with these lasso peptides makes them again sensitive to this drug. Taken together, our results suggest a possibility of an alternative direction in cancer therapy based on a combination of proliferation-inducing treatment and cytotoxic drugs targeting rapidly dividing cells.

Limitations of the Study

We note three limitations of this study. One relates to the exact mechanism of action of felipeptins on cancer cells, which appears to be due to the reduction in the amount of tumor suppressor protein Rb. However, how this reduction is achieved, and whether the felipeptins enter the cells or act on a membrane-anchored receptor is not known. Further studies, which would include more characterized cell lines, transcriptomics, and proteomics can clarify this issue. The second limitation is due to the low solubility of lasso peptides in water, which prevented the studies on complex formation in the aqueous solutions mimicking cellular environment. Hence, only formation of the complex in DMSO-based solution could be shown.

The third limitation relates to an idea of using the felipeptins in eukaryotic cell suspension cultures producing pharmaceutical proteins, where addition of lasso peptides could support more vigorous growth and hence increase the efficiency of the production process. This direction of research has not yet been addressed in the current study but deserves proper investigation.

Resource Availability

Lead Contact

Further information and requests for bacterial strains, constructs and materials should be directed to the Lead Contact, Prof. Sergey B. Zotchev (sergey.zotchev@univie.ac.at).

Materials Availability

Data related to this paper may be requested from the lead author. The bacterial strains isolated, constructed and examined in this study can be requested from the Lead Contact.

Data and Code Availability

The genome sequence of *Amycolatopsis* sp. YIM10 is available in GenBank under accession number CP045480.1. Chemical shift assignments of felipeptins A1 and A2 have been deposited in the BMRB under the accession codes 34,478 and 34,479, respectively. NMR ensemble structures of felipeptin A1and A2 are deposited in the Protein database under accession numbers 6TXH and 6TXI, respectively.

METHODS

All methods can be found in the accompanying Transparent Methods supplemental file.

SUPPLEMENTAL INFORMATION

Supplemental Information can be found online at https://doi.org/10.1016/j.isci.2020.101785.

ACKNOWLEDGMENTS

This study was supported by the University of Vienna, Swedish Research Council, Swedish Cancer Society, Bielefeld University, the University of Yunnan, NTNU Norwegian University of Science and Technology, and the grants from the Novo Nordisk Foundation (NNF18OC0032242) and the Norwegian Research Council (226244, 269408). We also acknowledge support by the Mass Spectrometry Center of the Faculty of Chemistry, University of Vienna.

AUTHORS CONTRIBUTION

S.B.Z., G.S., G.C., E.M., F.L.A. designed research; J.F.G.G., M.Z., M.S., S.R., E.U., Y.R.C., Y.J., G.C., E.M., F.L.A. performed research; M.Z., E.U., C.R., T.B., J.K., C.J., G.S., M.S., G.C., E.M., F.L.A. analyzed data; C.J. provided research material; S.B.Z., G.S., M.S., M.Z., C.J., G.C., E.M., F.L.A. wrote the paper.

DECLARATION OF INTERESTS

The authors declare no competing interest.

Received: July 9, 2020
Revised: October 16, 2020
Accepted: November 5, 2020
Published: December 18, 2020

REFERENCES

Allen, C.D., Chen, M.Y., Trick, A.Y., Le, D.T., Ferguson, A.L., and Link, A.J. (2016). Thermal unthreading of the lasso peptides Astexin-2 and Astexin-3. ACS Chem. Biol. *11*, 3043–3051.

Arnison, P.G., Bibb, M.J., Bierbaum, G., Bowers, A.A., Bugni, T.S., Bulaj, G., Camarero, J.A., Campopiano, D.J., Challis, G.L., Clardy, J., et al. (2013). Ribosomally synthesized and post-translationally modified peptide natural products: overview and recommendations for a universal nomenclature. Nat. Prod. Rep. *30*, 108–160.

Batlle, E., and Clevers, H. (2017). Cancer stem cells revisited. Nat. Med. *23*, 1124–1134.

Blin, K., Shaw, S., Steinke, K., Villebro, R., Ziemert, N., Lee, S.Y., Medema, M.H., and Weber, T. (2019). antiSMASH 5.0: updates to the secondary metabolite genome mining pipeline. Nucleic Acids Res. *47*, W81–W87.

Bloise, E., Ciarmela, P., Dela Cruz, C., Luisi, S., Petraglia, F., and Reis, F.M. (2019). Activin A in mammalian physiology. Physiol. Rev. *99*, 739–780.

Braffman, N.R., Piscotta, F.J., Hauver, J., Campbell, E.A., Link, A.J., and Darst, S.A. (2019). Structural mechanism of transcription inhibition by lasso peptides microcin J25 and capistruin. Proc. Natl. Acad. Sci. U S A *116*, 1273–1278.

Brown, J.A., Yonekubo, Y., Hanson, N., Sastre-Perona, A., Basin, A., Rytlewski, J.A., Dolgalev, I., Meehan, S., Tsirigos, A., Beronja, S., et al. (2017). TGF-β-Induced quiescence mediates chemoresistance of tumor-propagating cells in squamous cell carcinoma. Cell Stem Cell *21*, 650–664.

Brugarolas, J., Bronson, R.T., and Jacks, T.J. (1998). p21 is a critical CDK2 regulator essential for proliferation control in Rb-deficient cells. Cell Biol. *141*, 503–514.

Calcagno, A.M., Salcido, C.D., Gillet, J.P., Wu, C.P., Fostel, J.M., Mumau, M.D., Gottesman, M.M., Varticovski, L., and Ambudkar, S.V. (2010). Prolonged drug selection of breast cancer cells and enrichment of cancer stem cell characteristics. J. Natl. Cancer Inst. *102*, 1637–1652.

Chen, M., Wang, S., and Yu, X. (2019). Cryptand-imidazolium sup-ported total synthesis of the lasso peptide BI-32169 and its d-enantiomer. Chem. Commun. *55*, 3323–3326.

Cheung-Lee, W.L., Cao, L., Link, A.J., and Pandonodin, A. (2019). Proteobacterial lasso peptide with an exceptionally long C-terminal tail. ACS Chem. Biol. *14*, 2783–2792.

Choudhury, H.G., Tong, Z., Mathavan, I., Li, Y., Iwata, S., Zirah, S., Rebuffat, S., van Veen, H.W., and Beis, K. (2014). Structure of an antibacterial peptide ATP-binding cassette transporter in a novel outward occluded state. Proc. Natl. Acad. Sci. U S A *111*, 9145–9150.

de los Santos, E.L.C. (2019). NeuRiPP: neural network identi-fication of RiPP precursor peptides. Sci. Rep. *9*, 13406.

de Veer, S.J., Kan, M.W., and Craik, D.J. (2019). Cyclotides: from structure to function. Chem. Rev. *119*, 12375–12421.

DiCaprio, A.J., Firouzbakht, A., Hudson, G.A., and Mitchell, D.A. (2019). Enzymatic reconstitution and biosynthetic investigation of the lasso peptide fusilassin. J. Am. Chem. Soc. *141*, 290–297.

Fage, C.D., Hegemann, J.D., Nebel, A.J., Steinbach, R.M., Zhu, S., Linne, U., Harms, K., Bange, G., and Marahiel, M.A. (2016). Structure and mechanism of the Sphingopyxin I lasso peptide isopeptidase. Angew. Chem. Int. Ed. Engl. *55*, 12717–12721.

Gomez-Escribano, J.P., and Bibb, M.J. (2011). Engineering *Streptomyces coelicolor* for heterologous expression of secondary metabolite gene clusters. Microb. Biotechnol. *4*, 207–215.

Guo, Z.K., Zhang, G.F., Jiao, R.H., Shen, Y., Xu, Q., Tan, R.X., and Ge, H.M. (2012). Actinotetraoses A-H: tetrasaccharide derivatives from a grasshopper-associated *Amycolatopsis* sp. HCa1. Planta Med. *78*, 988–994.

Hanahan, D., and Weinberg, R.A. (2011). Hallmarks of cancer: the next generation. Cell *144*, 646–674.

Habault, J., and Poyet, J.L. (2019). Recent advances in cell pene-trating peptide-based anticancer therapies. Molecules *24*, E927.

Hegemann, J.D. (2020). Factors governing the thermal stability of lasso peptides. Chembiochem *21*, 7–18.

Hegemann, J.D., Zimmermann, M., Zhu, S., Klug, D., and Marahiel, M.A. (2013). Lasso peptides from proteobacteria: genome mining employing heterologous expression and mass spectrometry. Biopolymers *100*, 527–542.

Hegemann, J.D., Fage, C.D., Zhu, S., Harms, K., Di Leva, F.S., Novellino, E., Marinelli, L., and Marahiel, M.A. (2016). The ring residue proline 8 is crucial for the thermal stability of the lasso peptide caulosegnin II. Mol. Biosyst. *12*, 1106–1109.

Hegemann, J.D., Bobeica, S.C., Walker, M.C., Bothwell, I.R., and van der Donk, W.A. (2019). Assessing the flexibility of the prochlorosin 2.8 scaffold for bioengineering applications. ACS Synth. Biol. *8*, 1204–1214.

Jeanne Dit Fouque, K., Bisram, V., Hegemann, J.D., Zirah, S., Rebuffat, S., and Fernandez-Lima, F. (2019). Structural signatures of the class III lasso peptide BI-32169 and the branched-cyclic topoisomers using trapped ion mobility spectrometry-mass spectrometry and tandem mass spectrometry. Anal. Bioanal. Chem. *411*, 6287–6296.

Knappe, T.A., Linne, U., Xie, X., and Marahiel, M.A. (2010). The glucagon receptor antagonist BI-32169 constitutes a new class of lasso peptides. FEBS Lett. *584*, 785–789.

Koos, J.D., and Link, A.J. (2019). Heterologous and in vitro reconstitution of fuscanodin, a lasso peptide from *Thermobifida fusca*. J. Am. Chem. Soc. *141*, 928–935.

Li, Y., Ducasse, R., Zirah, S., Blond, A., Goulard, C., Lescop, E., Giraud, C., Hartke, A., Guittet, E., Pernodet, J.L., and Rebuffat, S. (2015a). Characterization of sviceucin from *Streptomyces* provides insight into enzyme exchangeability and disulfide bond formation in lasso peptides. ACS Chem. Biol. *10*, 2641–2649.

Li, Y., Zirah, S., and Rebuffat, S. (2015b). Lasso peptides. Bacterial Strategies to Make and Maintain Bioactive Entangled Scaffolds (Springer).

Maksimov, M.O., Pelczer, I., and Link, A.J. (2012). Precursor-centric genome-mining approach for lasso peptide discovery. Proc. Natl. Acad. Sci. U S A *109*, 15223–15228.

Martin-Gómez, H., Linne, U., Albericio, F., Tulla-Puche, J., and Hegemann, J.D. (2018). Investigation of the Biosynthesis of the Lasso Peptide Chaxapeptin Using an E. Coli-Based Production System. J. Nat. Prod. *81*, 2050–2056.

Martins-Neves, S.R., Cleton-Jansen, A.M., and Gomes, C.M.F. (2018). Therapy-induced enrichment of cancer stem-like cells in solid human tumors: where do we stand? Pharmacol. Res. *137*, 193–204.

Mevaere, J., Goulard, C., Schneider, O., Sekurova, O.N., Ma, H., Zirah, S., Afonso, C., Rebuffat, S., Zotchev, S.B., and Li, Y. (2018). An orthogonal system for heterologous expression of actinobacterial lasso peptides in *Streptomyces* hosts. Sci. Rep. *8*, 8232.

Morishita, Y., Chiba, S., Tsukuda, E., Tanaka, T., Ogawa, T., Yamasaki, M., Yoshida, M., Kawamoto, I., and Matsuda, Y. (1994). RES-701-1, a novel and selective endothelin type B receptor antagonist produced by *Streptomyces* sp. RE-701. I. Characterization of producing strain, fermentation, isolation, physico-chemical and biological properties. J. Antibiot. *47*, 269–275.

Pu, J., Wang, Q., Xu, W., Lu, L., and Jiang, S. (2019). Development of protein- and peptide-based HIV entry inhibitors targeting gp120 or gp41. Viruses *11*, E705.

Rosengren, K.J., Blond, A., Afonso, C., Tabet, J.C., Rebuffat, S., and Craik, D.J. (2004). Structure of thermolysin cleaved microcin J25: extreme stability of a two-chain antimicrobial peptide devoid of covalent links. Biochemistry *43*, 4696–4702.

Rycroft, D.S., Cole, W.J., and Rong, S. (1998). Highly oxygenated naphthalenes and acetophenones from the liverwort *Adelanthus decipiens* from the British isles and south America. Phytochemistry *48*, 1351–1356.

Takeishi, S., Matsumoto, A., Onoyama, I., Naka, K., Hirao, A., and Nakayama, K.I. (2013). Ablation of Fbxw7 eliminates leukemia-initiating cells by preventing quiescence. Cancer Cell *23*, 347–361.

Tietz, J.I., Schwalen, C.J., Patel, P.S., Maxson, T., Blair, P.M., Tai, H.C., Zakai, U.I., and Mitchell, D.A. (2017). A new genome-mining tool redefines the lasso peptide biosynthetic landscape. Nat. Chem. Biol. *13*, 470–478.

Um, S., Kim, Y.J., Kwon, H., Wen, H., Kim, S.H., Kwon, H.C., Park, S., Shin, J., and Oh, D.C. (2013). Sungsanpin, a lasso pep-tide from a deep-sea streptomycete. J. Nat. Prod. *76*, 873–879.

van Zundert, G.C.P., Rodrigues, J.P.G.L.M., Trellet, M., Schmitz, C., Kastritis, P.L., Karaca, E., Melquiond, A.S.J., van Dijk, M., de Vries, S.J., and Bonvin, A.M.J.J. (2016). The HADDOCK2.2 web server: user-friendly integrative modeling of biomolecular complexes. J. Mol. Biol. *428*, 720–725.

Wu, Q., Deering, R.W., Zhang, G., Wang, B., Li, X., Sun, J., Chen, J., Zhang, H., Rowley, D.C., and Wang, H. (2018). Albisporachelin, a new hydroxamate type siderophore from the deep ocean sediment-derived actinomycete *Amycolatopsis albispora* WP1T. Mar. Drugs *16*, E199.

Yan, K.P., Li, Y., Zirah, S., Goulard, C., Knappe, T.A., Marahiel, M.A., and Rebuffat, S. (2012). Dissecting the maturation steps of the lasso peptide microcin J25 in vitro. Chembiochem *13*, 1046–1052.

Zhu, S., Hegemann, J.D., Fage, C.D., Zimmermann, M., Xie, X., Linne, U., and Marahiel, M.A. (2016). Insights into the unique phosphorylation of the lasso peptide paeninodin. J. Biol. Chem. *291*, 13662–13678.

Zong, C., Wu, M.J., Qin, J.Z., and Link, A.J. (2017). Lasso peptide benenodin-1 is a thermally actuated [1]Rotaxane switch. J. Am. Chem. Soc. *139*, 10403–10409.

iScience, Volume *23*

Supplemental Information

Class IV Lasso Peptides Synergistically Induce Proliferation of Cancer Cells and Sensitize Them to Doxorubicin

Jaime Felipe Guerrero-Garzón, Eva Madland, Martin Zehl, Madhurendra Singh, Shiva Rezaei, Finn L. Aachmann, Gaston Courtade, Ernst Urban, Christian Rückert, Tobias Busche, Jörn Kalinowski, Yan-Ru Cao, Yi Jiang, Cheng-lin Jiang, Galina Selivanova, and Sergey B. Zotchev

Supplemental Information

Class IV lasso peptides synergistically induce proliferation of cancer cells and sensitize them to doxorubicin

Jaime Felipe Guerrero-Garzón, Eva Madland, Martin Zehl, Madhurendra Singh, Shiva Rezaei, Finn L. Aachmann, Gaston Courtade, Ernst Urban, Christian Rückert, Tobias Busche, Jörn Kalinowski, Yan-Ru Cao, Yi Jiang, Cheng-lin Jiang, Galina Selivanova*, Sergey B. Zotchev*

Transparent Methods

Isolation and taxonomic identification of Amycolatopsis *spp. YIM10. Amycolatopsis* sp. YIM10 was isolated from the soil sample collected in the rare earth mine of Bayan Obo, Inner Mongolia, China. The isolation medium contained (g/L): KH_2PO_4 - 1, KCl - 1, NH_4Cl - 1, $MgSO_4 \cdot 7H_2O$ - 0.24, $CaSO_4 \cdot 2H_2O$ - 0.17, NaCl - 25, sodium glutamate - 1, yeast extract - 5, casamino acids - 5, Na_2CO_3 – 5, agar – 20, pH 7-7.5. Total DNA extraction, PCR amplification of the 16S rRNA gene fragment was used according to earlier reported procedures (Bredholdt et al., 2007). Molecular taxonomy of the isolate was established using the analysis of the 16S rRNA gene sequence by the online "Classifier" tool of the Ribosomal Database Project (https://rdp.cme.msu.edu/classifier/classifier.jsp).

Bacterial strains, plasmids and growth conditions
Actinomycete strains were routinely maintained on Soya-Flour-Mannitol (SFM) agar plates at 28 °C (Flett et al., 1997). *Streptomyces coelicolor M1154* and *Streptomyces albus* J1074 were selected as heterologous expression hosts. *Escherichia coli* DH5α was selected as the host for cloning purposes, *E. coli* C was used as the host for Red/ET-mediated recombination and *E. coli* ET12567/pUZ8002 was used as the DNA donor strain in conjugation with *Streptomyces* strains (Gust, 2009). Plasmids, strains and primers used in this study are listed in Table S1. All the *E. coli* strains were grown overnight in LB medium at 200 rpm and 37 °C, except *E. coli* BW25113/pKD46 which requires 30 °C for the induction of the λ RED recombination system.

Cultivation of Amycolatopsis spp. YIM10 and purification of secondary metabolites. 15 mL of TSB medium (Oxoid, UK) was inoculated with 200 µL of a dense spore suspension of isolate YIM10 in a 100 mL Erlenmeyer flask and incubated at 28 °C with 200 rpm for 10 days to produce a seed culture. For the purification of 1,2,4-trimethoxynaphthalene, 250 mL of medium 5288 (Soy flour 10 g, Glycerol 15 g, NaCl 5 g, $CaCO_3$ 1 g, $CoCl_2 \cdot 7H_2O$ 1mg, in 1 L of distilled water) were inoculated with 30 mL of seed culture stock and fermented in 2 L baffled Erlenmeyer flasks at 28 °C with 200 rpm for 14 days. The whole culture was freeze-dried and extracted with 150 mL of methanol for 1 hour. The organic phase was evaporated in vacuo to generate a dry layer. The crude extract (500 mg) was mixed with Silica gel 60 from MERCK (particle size 0.063–0.200 nm for column chromatography) in a proportion 1:2 and packaged in cartridge. For fractionation the PuriFlash column 15 C18 HQ 35G−35.0 g (22 bar) was used with a gradient of 5–98% Methanol/H_2O in 50 min and a flow of 15 mL/min using a PuriFlash 420 instrument. Forty-two fractions were obtained and pooled into 16 main fractions, which were freeze dried, and concentrated in methanol for antimicrobial bioassays. Fraction F11 (fractions 30-31) resulted in approximately 4 mg of pure substance (1,2,4-Trimethoxynaphthalene) which was analyzed by LC-MS, direct infusion HRESIMS and 1D and 2D NMR methods (^{1}H-NMR, ^{13}C-NMR, HSQC, HMBC and COSY).
For the purification of tigloside, 500 mL of medium 5288 were inoculated with 30 mL of seed culture stock and fermented in 2 L baffled Erlenmeyer flasks at 28 °C with 200 rpm for 14 days. The culture was centrifuged for 10 min at 4000 rpm and room temperature. The pellet was extracted with 300 mL of pure methanol for 1 hour using 100 rpm at room temperature. The methanolic extract was concentrated in vacuo. 2 mL of crude extract was separated using a Hibar® 250-25 LiChrospher® 100 RP-18e, 5 µm column (Merck) in a semi-preparative HPLC (Shimadzu LC-8A). 0.1% aqueous formic acid and acetonitrile were used as mobile phase A and B, respectively. The gradient used was: 42–65% B in 46 min followed by a washing (10 min, 95% B) and re-equilibration step (10 min, 42% B), using a flow rate of 15.5 mL/min and a detection wavelength of 190 nm. Tigloside eluted with a retention time of approximately 30 min. Around 10 mg of pure substance were purified and analyzed by LC-MS, direct infusion HRESIMS and 1D and 2D NMR methods (^{1}H-NMR, ^{13}C-NMR, HSQC, HMBC and COSY).

LC-MS, HRESIMS and NMR analysis. LC-MS analyses of the methanolic extract of the *Amycolatopsis* spp. YIM10 culture and relevant fractions thereof were performed on a maXis HD ESI-Qq-TOF mass spectrometer (Bruker Daltonics, Bremen, Germany) that was connected to an UltiMate 3000 RSLC-series system

(Dionex/Thermo Fisher Scientific, Germering, Germany). Separation was carried out on an Acclaim 120 C18, 2.1 x 150 mm, 3 µm HPLC column (Thermo Fisher Scientific) using water and acetonitrile, both modified with 0.1 % formic acid, as mobile phase A and B, respectively. The sample components were separated and eluted with a linear gradient from 5% to 95% B in 45 min followed by an isocratic column cleaning (10 min at 95 % B) and re-equilibration step (10 min at 5 % B). The flow rate was 0.45 mL/min and the column oven temperature was set to 25 °C. After passing the UV detector, the eluate flow was split approximately 1:8 and high-resolution MS spectra were recorded in positive ion mode in the range m/z 50-3000. The following ESI ion source settings were applied: capillary voltage: 4.5 kV, nebulizer: 0.8 bar (N_2), dry gas flow: 7.0 L/min (N_2), and dry temperature: 200 °C. The sum formulas of the detected ions were determined using Bruker Compass DataAnalysis 4.2 based on the mass accuracy ($\Delta m/z \leq 5$ ppm) and isotopic pattern matching (SmartFormula algorithm). Direct infusion HRESIMS and HRESIM/MS spectra were also recorded on the maXis HD ESI-Qq-TOF instrument under individually optimized conditions.

NMR analysis of tiglosides and 1,2,4-trimethoxynaphthalene. NMR spectra were recorded on a Bruker Avance 500 NMR spectrometer (UltraShield) using a 5 mm probe (TCI Prodigy cryogenic probe) with z-axis gradients and automatic tuning and matching accessory (Bruker BioSpin). The resonance frequency for ^{1}H NMR was 500.13 MHz and for ^{13}C NMR 125.75 MHz. All measurements were performed for a solution in fully deuterated methanol at 25 ^{o}C. Standard 1D and gradient-enhanced (ge) 2D experiments, like double quantum filtered (DQF) COSY, HSQC, and HMBC, were used as supplied by the manufacturer. Chemical shifts are referenced internally to the residual, non-deuterated solvent signal for methanol ^{1}H (δ 3.31 ppm) and to the carbon signal of the solvent for methanol ^{13}C (δ 49.00 ppm).

Genome sequencing and analyses. To obtain the complete genome sequence of *Amycolatopsis* sp. YIM10, two WGS sequencing libraries were prepared, using the TruSeq DNA PCR-Free Kit respectively the Nextera Mate Pair Library Preparation Kit (Illumina Inc., San Diego, CA, U.S.A.) according to the manufacturer's instructions. The resulting libraries were sequenced on the MiSeq sequencing platform using the MiSeq Reagent Kit v3 in a 2x 300Â nt sequencing run. The sequencing data sets were assembled using the Newbler assembler v2.8 (454 Life Sciences, Branford, CT, U.S.A.). The initial assembly consisted of 4 scaffolds larger than 2 kbp containing 78 contigs, with an additional 39 smaller contigs that were not assigned to scaffolds. The assembly was then manually curated in Consed (Gordon and Green, 2013). The remaining three gaps were closed by PCR and Sanger sequencing, resulting in a single contig for the circular chromosome. An additional contig represented a phage genome which apparently is present in two forms: integrated in the genome and as a circular episome. The assembled contigs were annotated using the Prokka pipeline v1.11 (Seemann, 2014). This resulted in the detection and annotation of 9,612 CDS, 71 tRNAs, 12 rRNAs, and 32 ncRNAs.

Genomic library construction and screening. For constructing a genome library of *Amycolatopsis* sp. YIM10, the CopyControl™ Fosmid Library Production Kit with pCC1FOS™ Vector (Epicentre) was used according to the established protocol. ca. 1200 clones were picked, transferred into 96-well plates and stored at -80 °C. Three primer pairs were designed to amplify flanking and central regions of the targeted cluster (Table S2). Screening of the library was done using pooled PCR (Israel, 2006) to identify the desired BGC, which occurred in a single fosmid.

Construction of recombinant strains for heterologous production of felipeptins. The fosmids pCC1FOS-Cluster 21, pCC1FOS-Cluster 12 and pCC1FOS-Putative tigloside cluster were first individually transferred into the *E. coli* BW25113/pKD46 strain. Then a neo- int-attP$^{\varphi C31}$ (6.645 kb) cassette was used to replace the chloramphenicol resistance gene on fosmids via Red/ET-mediated recombination (Gust, 2009). The modified fosmids were transferred into *E. coli* ET12567/pUZ8002 and transferred into *S. coelicolor* M1154 and *S. albus* J1074, respectively, using conjugation. Plasmid pSET152 (int-attP$^{\varphi C31}$) was used as a control for conjugation and as negative control in further analysis of lasso peptide production. Kanamycin (50 µg/mL) was used for selection of recombinant *Streptomyces* strains.
The DNA fragment (1.5 kb), containing the SARP regulator gene, identified in cluster 21, was amplified by PCR using gDNA of *Amycolatopsis* sp. YIM10 as template using primers SARP_Fw and SARP_Rv (Table S2). These primers included the restriction sites *Eco*RI and *Eco*RV respectively, to allow proper cloning in pSOK806 plasmid (Sekurova et al., 2016). The resulting construct was introduced in the *S. coelicolor* M1154 and *S. albus* J1074 containing the integrated pCC1FOS-Cluster 21 fosmid via conjugation from *E. coli* ET12567/pUZ8002.
Apramycin (50 µg/mL) was used for selection of the recombinant *Streptomyces* strains.
Oligonucleotide primers were designed using Clone Manager 9 software (Sci-Ed Software, USA). The flanking regions for each construct were sequenced.

Production and purification of felipeptins A1 and A2. 100 mL flasks containing 10 mL of YEME medium (yeast extract 3 g/L, peptone 5 g/L, malt extract 3 g/L, glucose 10 g/L, sucrose 340 g/L) were inoculated with 200 µL of *Streptomyces coelicolor* M1154_pCC1-FOS-Cluster 21_pSOK806-SARP strain spore suspension. The cultures

were incubated at 200 rpm and 28 °C for 5 days. Then, 250 mL baffled flasks containing 50 mL of YEME medium were inoculated with 3 mL of the well grown cultures above mentioned. The cultures were incubated at 200 rpm and 28 °C for 3 days until dense growth was obtained to generate a seeding culture. 2 L baffled flasks containing 500 mL of MYM medium (4 g/L maltose, 4 g/L yeast extract, 10 g/L malt extract, 1.9 g/L MOPS) were inoculated with 20 mL of seeding culture. The fermentation was carried out at 200 rpm and 28 °C for 7 days, after which the cultures were harvested and freeze dried. 300 mL of methanol plus 6 % formic acid were used to extract the freeze dried material. Extraction was carried out at 200 rpm at room temperature for 3 hours. The methanolic extract was centrifuged at 400 rpm at room temperature for 10 min to get rid of debris before being concentrated under reduced pressure in a minimum volume of methanol (from 300 to 15 mL approximately). 1 mL of formic acid was added per 50 mL of concentrated methanol extract. Then, the extract was transferred to 20 mL 1 kDa MWCO Mega Pur-A-Lyzer kit (Sigma-Aldrich) tubes for dialysis against 2 L of buffer solution (50 mM sodium phosphate, 100 mM NaCl, pH 8.0) during 2 days at 4 °C with slowly stirring. After dialysis, the material was centrifuged at 10,000 rpm and 4 °C for 10 minutes. The pellet was dissolved in methanol plus 6% formic acid. The methanolic extract was separated using a Shim-pack GIS C18, 250 mm x 20 mm, 5 µm column (Shimadzu) in a Semi-preparative HPLC Shimadzu LC-20AR equipment. 0.1% aqueous formic acid and acetonitrile were used as mobile phase A and B, respectively. The gradient used was: 10–55% B in 20 min followed by a washing (10 min at 95% B) and re-equilibration step (10 min at 10% B), flow rate was 20 mL/min and 190 nm wavelength was used for detection. Felipeptin A1 eluated with a retention time of 14 minutes, and felipeptin A2 with retention time of 11 minutes. Approximately 12 mg of felipeptin A1 and 7 mg of felipeptin A2 were yielded per liter of fermentation culture.

The LC-MS analyses of the extracts and fractions containing the lasso peptides were performed on an UltiMate 3000 series system HPLC equipped with a VWD detector (Dionex/Thermo Fisher Scientific) that was coupled to a maXis UHR ESI-Qq-TOF mass spectrometer (Bruker Daltonics). Separation was carried out on an Acclaim 120 C18, 2.1 x 150 mm, 3 µm HPLC column as described above. After passing the UV detector, high-resolution MS and MS/MS spectra were recorded in positive ion mode in the range m/z 50-3000. The following ESI ion source settings were applied: capillary voltage: 4.5 kV, nebulizer: 1.2 bar (N_2), dry gas flow: 8.0 L/min (N_2), and dry temperature: 180 °C. MS/MS spectra were obtained in automated data-dependent acquisition mode using argon as collision gas, an isolation window of $\Delta m/z = 4$, and an m/z- and charge-dependent fragmentation amplitude. The data shown in Figure S9 were obtained with an LTQ Orbitrap Velos mass spectrometer coupled to a Vanquish Horizon UHPLC system (both from Thermo Fisher Scientific) under identical chromatographic conditions.

NMR spectroscopy of felipeptin A1 and A2. To prepare the felipeptins for NMR, freeze-dried felipeptins were placed in an exicator with silica gel for ~2 hours to remove residual water before dissolving 0.5-1.2 mg felipeptin A1 or A2 in 160-180 µL DMSO-d_6 (99.9% D; Isotec, USA). Despite our efforts, felipeptins were poorly soluble in other solvent systems (water; 95% methanol-d_4 (99.8% D; CIL, USA) with 5% formic acid-d_2 (99%+ D, Sigma-Aldrich/Merck).

Hereafter, the samples were transferred to a 3 mm NMR tube. All homo- and heteronuclear NMR spectra were recorded on a Bruker Ascend 800 MHz Avance III HD NMR spectrometer (Bruker BioSpin AG, Fälladen, Switzerland) equipped with 5 mm with cryogenic CP-TCI probe. All NMR recording were performed at 25 °C. The chemical shifts were calibrated by using he residual DMSO signal. For the chemical shift assignment, the following spectra were recorded: 1D proton, 2D double quantum filtered correlation spectroscopy (DQF-COSY), 2D total correlation spectroscopy (TOCSY) with 70 ms mixing time, 2D nuclear Overhauser effect correlation spectroscopy (NOESY) with 100 ms mixing time, 2D ^{13}C heteronuclear single quantum coherence (HSQC) with multiplicity editing, 2D ^{13}C HSQC-[^1H,^1H]TOCSY with 70 ms mixing time on protons, 2D heteronuclear multiple bond correlation (HMBC) with BIRD filter to suppress first order correlations and 2D ^{15}N HSQC. The spectra were recorded, processed and analyzed using TopSpin 3.5 software (Bruker BioSpin) and CARA (Keller, 2004). The chemical shift assignments have been deposited in the BioMagResBank under the accession numbers 34478 (A1) and 34479 (A2). Structures were calculated in CYANA (Güntert, 2004) using 264 (A1) and 188 (A2) NOE-derived distance restraints, as well as a disulfide bond (Cys13-Cys17) and restraints for the isopeptide bond between Gly1 and Glu8. To remove bumps and correct the covalent geometry, the structures were energy-minimized in YASARA (Krieger et al., 2002) with the NOVA force field, and the Particle Mesh Ewald algorithm (Essmann et al., 1995) to treat long range electrostatic interactions. After removal of conformational stress by a short steepest descent minimization, the procedure continued by simulated annealing (timestep 2 fs, atom velocities scaled down by 0.9 every 10th step) until the energy improved by less than 0.05 kJ/mol per atom during 200 steps. The CYANA target function was calculated 4.42 ± 0.29 Å^2 (A1) and 3.91 ± 0.37 Å^2 (A2), as was the backbone (N, C^α, C') rmsd 0.88 ± 0.40 Å (A1) and 0.88 ± 0.21 Å (A2). The structural ensembles have been deposited in the Protein DataBank under the accession codes 6TXH (A1) and 6THI (A2).

The interaction between felipeptin A1 and A2 was investigated using NMR titration. A ^{13}C-HSQC spectrum of 1.15 mM felipeptin A2 in 160 µL DMSO-d_6 was recorded at 25 °C as reference. New spectra were recorded after addition of felipeptin A1 (0.29, 0.56, 1.10, 1.52, 1.86, 2.14, 2.38, 2.50 and 5.00 mM). A ^{15}N-HSQC spectrum was recorded with both felipeptins added in a 1:1 ratio (~1.2 mM). The chemical shift perturbation δ_{CS} (in ppm) was

calculated from the series of ^{13}C-HSQC spectra using Equations 5 and 9 from Krishnamoorthy et al (2010). A HADDOCK model (Di Veroli et al., 2016) of the interaction was generated using the Easy Interface of the HADDOCK webserver (https://haddock.science.uu.nl/services/HADDOCK2.2/haddockserver-easy.html). Amino acids where at least one atom had δ_{CS} larger than the average δ_{CS} plus one standard deviation were defined as "active residues" (A1: 15,17; A2: 5,7,11,12,14,15); whereas "passive residues" were automatically assigned by HADDOCK.

Antimicrobial activity testing. The antibacterial activity of pure compounds, fractions and crude extracts were initially tested using the disk diffusion assay with *Bacillus subtilis* 168 as test organism. Additionally, liquid assays procedures were used to determine the antimicrobial activity of felipeptin A1, felipeptin A2 and their combination (1:1) against a panel of 10 Gram positive pathogens: *Staphylococcus aureus* MRSA MB5393, *Staphylococcus aureus* MSSA ATCC29213, *Staphylococcus epidermidis* (Clinical isolate linezolid resistant), *Enterococcus faecium* (Clinical isolate vancomycin sensitive-1), *Enterococcus faecium* (Clinical isolate VanA resistant), *Enterococcus faecium* (Clinical isolate VanB resistant), *Enterococcus gallinarum* (Clinical isolate VanC resistant), *Streptococcus mutans* ATCC25 175, *Streptococcus pyogenes* (Clinical isolate sensitive) and *Streptococcus pneumonia* ATCC49619 (penicillin medium resistance). MIC assays were done by MEDINA Foundation (Granada, Spain). Compounds were tested in a liquid growth medium dispensed in 96 plates inoculated with a standardized bacterial suspension (CFU/ Following overnight incubation at 37 °C, the plates were examined for bacterial growth as evidenced by turbidity.

Bioassays on human cell lines. BJ normal fibroblasts, MCF7, HCT116 and A375 (ATCC) were cultured in DMEM supplemented with 10% FBS (Hyclone), 2 mM L-glutamine, 100 U/ml of penicillin and 100 mg/ml of streptomycin (Sigma-Aldrich). CRISPR/Cas9-mediated p53 deletion was performed in stable Cas9 expressing MCF7 and A375 as previously described ()Peuget et al., 2020). Bone-marrow derived mesenchymal stem cells (MSC) kindly provided by Dr. Muhammad Mushtaq (Karolinska Institutet) were cultured in mesenchymal stem cells medium recommended by ATCC. All cells were kept under 37°C with 5% CO_2 incubation.

Compounds. Felipeptins A1 and A2 were dissolved in DMSO and doxorubicin (Sigma-Aldrich) was dissolved in water. The compounds concentrations used in a particular experiment are indicated in the figure legends.

Felipeptins combination treatment and combination index calculation. Approximately 2000-3000 cells were seeded in 96-well plates (Sigma-Aldrich) and treated with a different concentration of felipeptins A1 and A2 for 72 hours. For doxorubicin treatment cells pre-incubated with felipeptins or not were treated with indicated doxorubicin concentration for another 72h. Cell viability was assessed using a resazurin assay according to manufacturer's instructions. Data analysis were performed using Excel and mean values were presented as heatmaps via Morpheus (https://software.broadinstitute.org/morpheus). Combenefit software was used to calculate combination index (Krishnamoorthy et al., 2010), where an HSA model was applied for synergism definition and displayed as heatmaps via online Morpheus software (https://software.broadinstitute.org/morpheus/).

Long-term colony formation assay. 1000 A375 cells were seeded in each well of 12 well plates. The next day, the medium was removed and 1ml of medium containing a combination of felipeptins A1 and A2 (6.25 µM FA1 and 12.5 µM FA2) was added in the respective wells and the plates were incubated at 37°C with 5% CO_2 for 72h before treatment with 0.05 or 0.1 µM doxorubicin for another 72 hours. The colonies were stained using crystal violet and captured using capture device.

Generation of doxorubicin-resistant cells followed by treatment with felipeptins. Generation of doxorubicin resistant cancer stem cells was performed as described elsewhere (Calcagno et al., 2010). Briefly, 500 MCF7 cells were treated with low dose of doxorubicin (12.5 nM) in 12-well plates for 72h. To stimulate the growth of doxorubicin-resistant cells they were incubated with felipeptins A1 and A2 (25 µM each) for another 96h. Obtained colonies were treated with same concentrations of felipeptins and doxorubicin for another 5 days, stained with crystal violet and quantified using Image J analysis.

Cell cycle analysis. Cell cycle analysis was performed using propidium-iodide staining (Thermo Scientific) and Flow Cytometry. In brief, cells were treated with felipeptins (6,25 µM or 12.5 µM each) for 24h, harvested, ethanol fixed at -20C and analyzed by FACSCalibur (BD Biosciences). Cell cycle analysis was performed by Cell Quest software (BD Biosciences).

Protein extraction and Western blotting. A375 cells were plated in 6cm plates at 40% confluency. The following day, cells were treated with either DMSO or a combination of felipeptins (6,25 µM or 12.5 µM each) for 24h. Cells were lysed on ice using RIPA buffer (25 mM Tris-HCl pH 7.6, 150 mM NaCl, 1% Triton-X-100, 0.1% sodium deoxycholate, 0.1% SDS), containing protease and phosphatase inhibitors for 20-30 min, interspersed with brief

vortexing. The nonsoluble fraction was removed by centrifugation and the protein concentration was measured in supernatant using a BCA kit according to manufacturer's protocol (Thermo Scientific).
Fifteen 15 µg of protein was separated by SDS-PAGE and transferred onto a 0.45 µm nitrocellulose membrane (GE Healthcare). The membrane was blocked using 5% milk and incubated with the primary anti-total Rb antibody (#9309, Cell Signaling Technology) and anti-phospho-Rb (Ser807/811, #8516, Cell Signaling Technology) overnight at 4˚C. On the following day, the membranes were washed with 1X PBST (3X5 min) and incubated with the appropriate Goat-anti-mouse HRP-labeled secondary antibody (Jackson ImmunoResearch) and SuperSignal™ West Dura Extended Duration Substrate detection system (Thermo Fischer Scientific), and images were visualized using ChemiDoc Imaging System (Bio-Rad). β-actin, detected using anti-β-actin monoclonal antibody (Millipore) was used as loading control.

Supplemental Figures

Figure S1. HRESIMS/MS spectra of the $[M+H]^+$ ion of 1,2,4-trimethoxynaphthalene at *m/z* 219.1016 in the active fraction F11 of the methanol crude extract from *Amycolatopsis* sp. YIM10. The CID spectra were obtained with collision energies of 21 eV (A) and 35 eV (B).

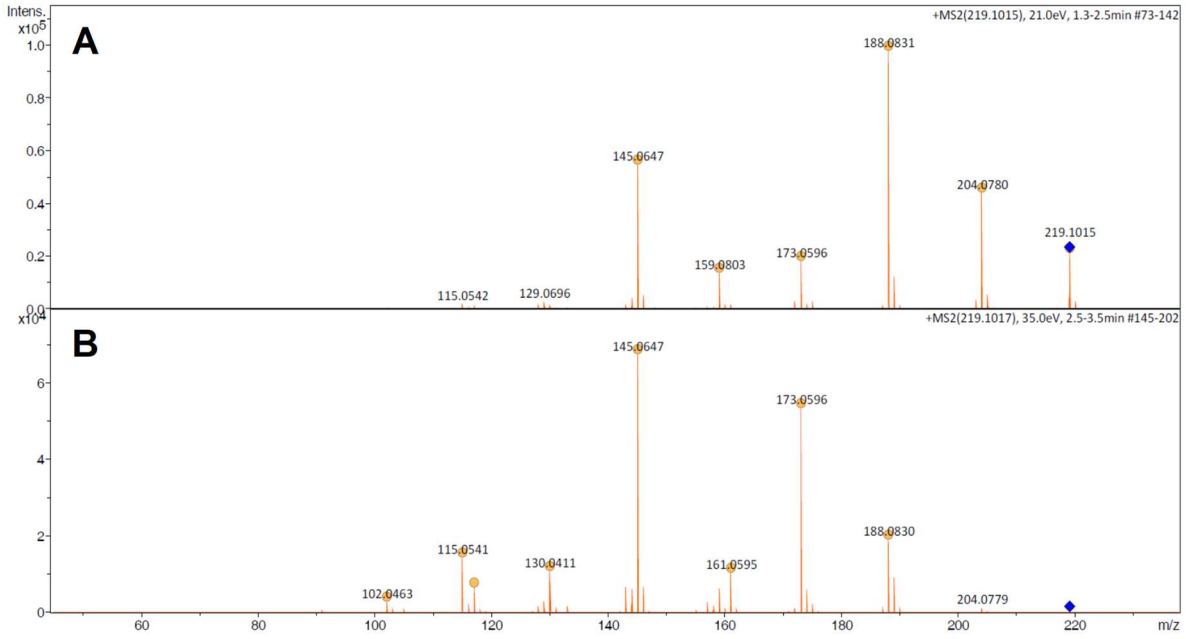

Figure S2. LC-HRESIMS spectrum of the preparative HPLC fraction F8 of the methanol crude extract from *Amycolatopsis* sp. YIM10 cultivated in 5288 medium. The close-up shows the measured isotopic pattern of the $[M+2H]^{2+}$ ion of tigloside at m/z 580.2435 (A) in comparison to the calculated isotopic pattern for an ion with the sum formula $C_{54}H_{80}O_{27}^{2+}$ (B).

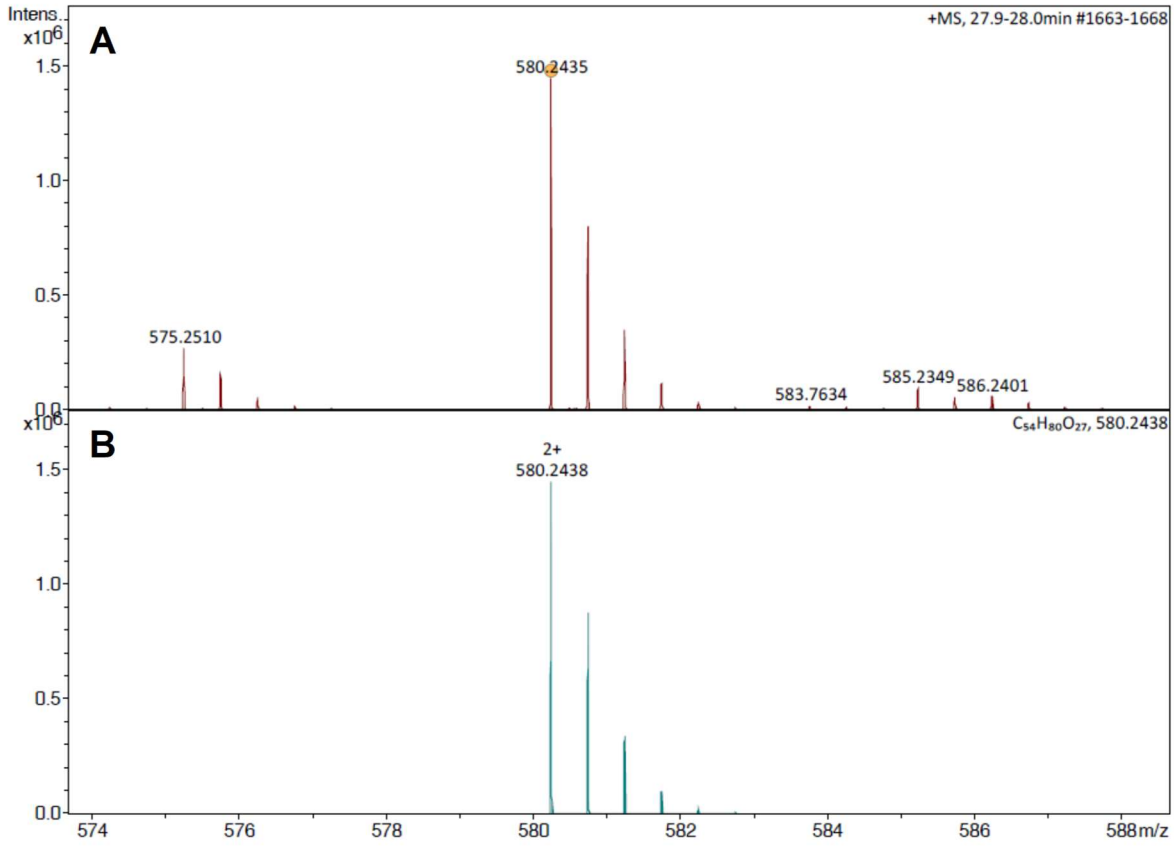

Figure S3. HRESIMS/MS spectrum of the $[M+H]^+$ ion of tigloside at *m/z* 1159.4791 in the preparative HPLC fraction F8 of the methanol crude extract from *Amycolatopsis* sp. YIM10. The CID spectrum was obtained with a collision energy of 15 eV.

Acquisition Parameter

Source Type	ESI	Ion Polarity	Positive	Set Nebulizer	0.4 Bar
Focus	Active	Set Capillary	1500 V	Set Dry Heater	200 °C
Scan Begin	50 m/z	Set End Plate Offset	-500 V	Set Dry Gas	4.0 l/min
Scan End	1550 m/z	Set Charging Voltage	2000 V	Set Divert Valve	Waste
		Set Corona	0 nA	Set APCI Heater	0 °C

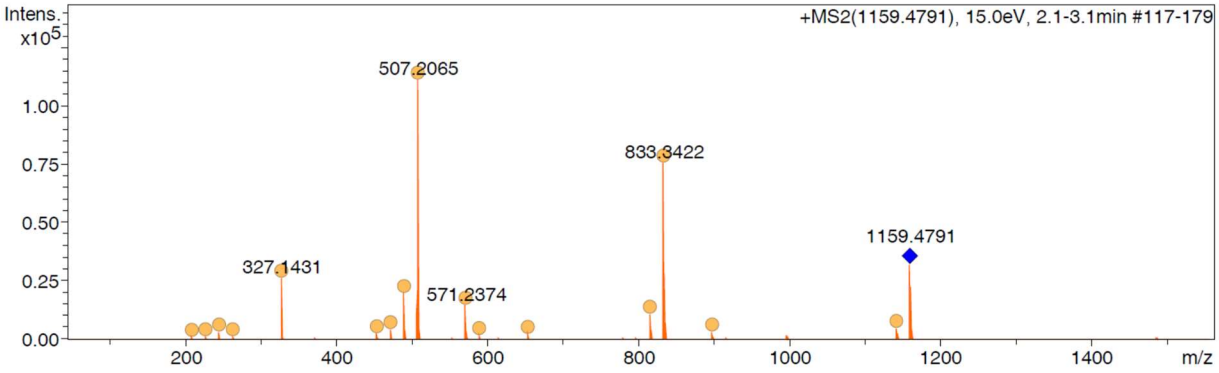

Meas. m/z	#	Ion Formula	m/z	err [ppm]	mSigma	# mSigma	Score	rdb	e⁻ Conf	N-Rule
209.0802	1	C11H13O4	209.0808	2.9	9.0	1	100.00	5.5	even	ok
227.0908	1	C11H15O5	227.0914	2.7	17.3	1	100.00	4.5	even	ok
245.1014	1	C11H17O6	245.1020	2.3	18.5	1	100.00	3.5	even	ok
263.1118	1	C11H19O7	263.1125	2.7	14.5	1	100.00	2.5	even	ok
327.1431	1	C16H23O7	327.1438	2.2	14.4	1	100.00	5.5	even	ok
453.1745	1	C22H29O10	453.1755	2.4	27.2	1	100.00	8.5	even	ok
471.1852	1	C22H31O11	471.1861	1.9	19.0	1	100.00	7.5	even	ok
489.1956	1	C22H33O12	489.1967	2.2	13.7	1	100.00	6.5	even	ok
507.2065	1	C22H35O13	507.2072	1.3	14.9	1	100.00	5.5	even	ok
571.2374	1	C27H39O13	571.2385	1.9	20.6	1	100.00	8.5	even	ok
589.2476	1	C27H41O14	589.2491	2.5	38.5	1	100.00	7.5	even	ok
653.2791	1	C32H45O14	653.2804	1.9	28.9	1	100.00	10.5	even	ok
815.3316	1	C38H55O19	815.3332	2.0	24.0	1	100.00	11.5	even	ok
833.3422	1	C38H57O20	833.3438	1.9	29.5	1	100.00	10.5	even	ok
897.3732	1	C43H61O20	897.3751	2.0	42.1	1	100.00	13.5	even	ok
1141.4673	1	C54H77O26	1141.4698	2.1	39.5	1	100.00	16.5	even	ok

Figure S4. HRESIMS/MS spectrum of the $[M+2H]^{2+}$ ion of tigloside at *m/z* 580.2434 in the preparative HPLC fraction F8 of the methanol crude extract from *Amycolatopsis* sp. YIM10. The CID spectrum was obtained with a collision energy of 8 eV.

Acquisition Parameter

Source Type	ESI	Ion Polarity	Positive	Set Nebulizer	0.4 Bar
Focus	Active	Set Capillary	1500 V	Set Dry Heater	200 °C
Scan Begin	50 m/z	Set End Plate Offset	-500 V	Set Dry Gas	4.0 l/min
Scan End	1550 m/z	Set Charging Voltage	2000 V	Set Divert Valve	Waste
		Set Corona	0 nA	Set APCI Heater	0 °C

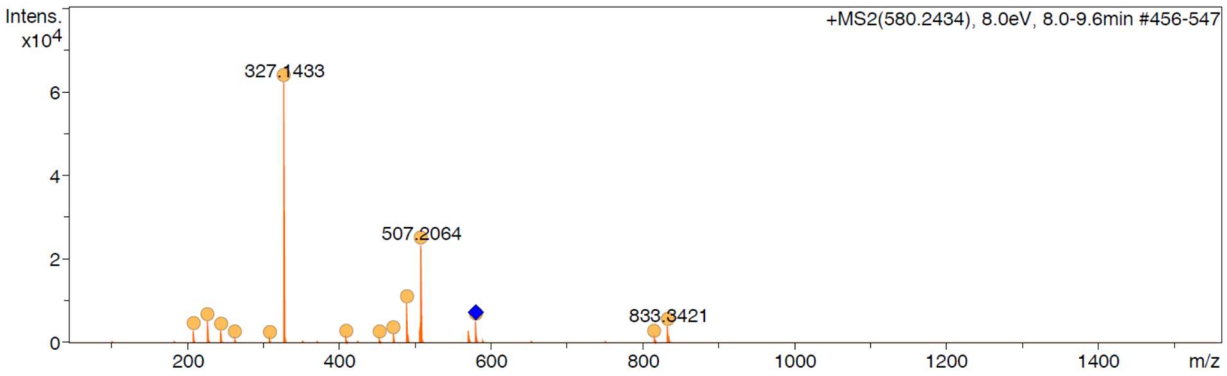

Meas. m/z	#	Ion Formula	m/z	err [ppm]	mSigma	# mSigma	Score	rdb	e⁻ Conf	N-Rule
209.0803	1	C11H13O4	209.0808	2.7	11.4	1	100.00	5.5	even	ok
227.0909	1	C11H15O5	227.0914	2.3	11.2	1	100.00	4.5	even	ok
245.1014	1	C11H17O6	245.1020	2.3	17.3	1	100.00	3.5	even	ok
263.1121	1	C11H19O7	263.1125	1.8	13.3	1	100.00	2.5	even	ok
309.1328	1	C16H21O6	309.1333	1.6	16.5	1	100.00	6.5	even	ok
327.1433	1	C16H23O7	327.1438	1.6	12.2	1	100.00	5.5	even	ok
409.1849	1	C21H29O8	409.1857	1.9	29.3	1	100.00	7.5	even	ok
453.1746	1	C22H29O10	453.1755	2.0	25.0	1	100.00	8.5	even	ok
471.1853	1	C22H31O11	471.1861	1.6	28.3	1	100.00	7.5	even	ok
489.1958	1	C22H33O12	489.1967	1.7	10.8	1	100.00	6.5	even	ok
507.2064	1	C22H35O13	507.2072	1.6	10.9	1	100.00	5.5	even	ok
580.2434	1	C54H80O27	580.2438	0.7	14.9	1	100.00	15.0	even	ok
815.3315	1	C38H55O19	815.3332	2.1	17.1	1	100.00	11.5	even	ok
833.3421	1	C38H57O20	833.3438	2.0	18.7	1	100.00	10.5	even	ok

Figure S5. NMR datasheet for 1,2,4-Trimethoxynaphthalene, $C_{13}H_{14}O_3$ (m/e = 218,25)

GF10_F11B in d_4Methanol		^{1}H	^{13}C
1	C	--	137,30
2	C	--	149,59
3	CH	6,81	96,27
4	C	--	153,91
4a	C	--	122,50
5	CH	8,10	123,08
6	CH	7,31	124,26
7	CH	7,46	127,89
8	CH	7,97	121,68
8a	C	--	130,35
OCH_3 at 1	CH_3	3,88	61,57
OCH_3 at 2	CH_3	4,00	57,65
OCH_3 at 4	CH_3	4,01	56,32

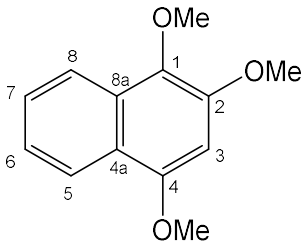

Figure S6. NMR datasheeta for tiglosides: $C_{54}H_{78}O_{27}$ (m/e = 1158.47)

GF10_F8 in d_4Methanol		^{1}H	^{13}C
COO at 6	C	--	169,44
COO at 3'	C	--	168,79
COO at 4'	C	--	168,20
CH at 4'	CH	6,81	140,02
CH at 3'	CH	6,83	139,31
CH at 6	CH	6,93	138,97
CH_3 at 6	C	--	129,67
CH_3 at 3'	C	--	129,24
CH_3 at 4'	C	--	129,93
1	CH	5,31	95,73
2	CH	3,67	81,58
3	CH	3,93	73,87
4	CH	3,57	71,13
5	CH	4,21	71,17
6	CH_2	4,55/4,35	63,88
1'	CH	4,71	105,79
2'	CH	3,51	73,79
3'	CH	5,25	76,22
4'	CH	4,92	70,82
5'	CH	3,66	76,22
6'	CH_2	3,59	62,38
CH_3(d) at 3'	CH_3	1,78	14,48
CH_3(d) at 4'	CH_3	1,78	14,48
CH_3(s) at 6	CH_3	1,87	14,43
CH_3(d) at 6	CH_3	1,83	12,30
CH_3(s) at 3'	CH_3	1,78	12,15
CH_3(s) at 4'	CH_3	1,75	12,07

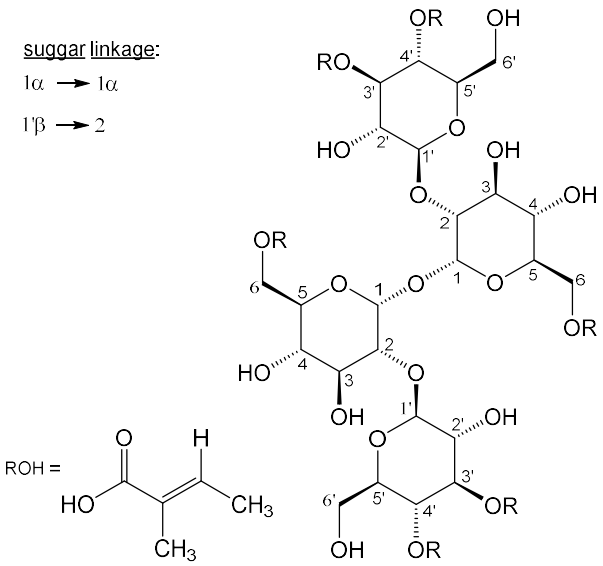

GF10_F8 in d_4Methanol	coupling in Hz
1 - 2	2,3
2 - 3	9,3
3 - 4	9,3
4 - 5	9,9
5 – 6/1	-
5 – 6/2	-
6/1 – 6/2	11,9
1' - 2'	7,7
2' - 3'	9,5
3' - 4'	9,5
4' - 5'	?
5' – 6/1'	-
5' – 6/2'	-
6/1' – 6/2'	-

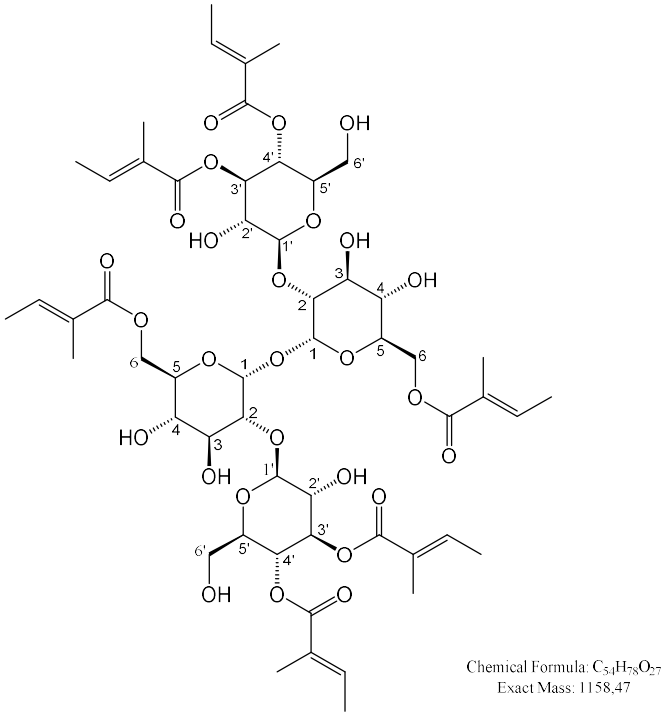

Figure S7. LC-MS monitoring of the heterologous expression of felipeptin A1 and A2, Related to Figure 1. Positive ion mode base peak chromatograms (*m/z* 50-3000) of extracts from *Streptomyces* M1154 recombinant strains carrying the plasmid pSET152 (A), the lasso peptide cluster 21 (B), the lasso peptide cluster 21 and the pSOK806 plasmid (C), and the lasso peptide cluster 21 overexpressing the SARP regulator gene *filR1*. The strains were cultivated in MYM medium. The lasso peptides felipeptin (FP) A1 and A2 are only produced in the latter strain.

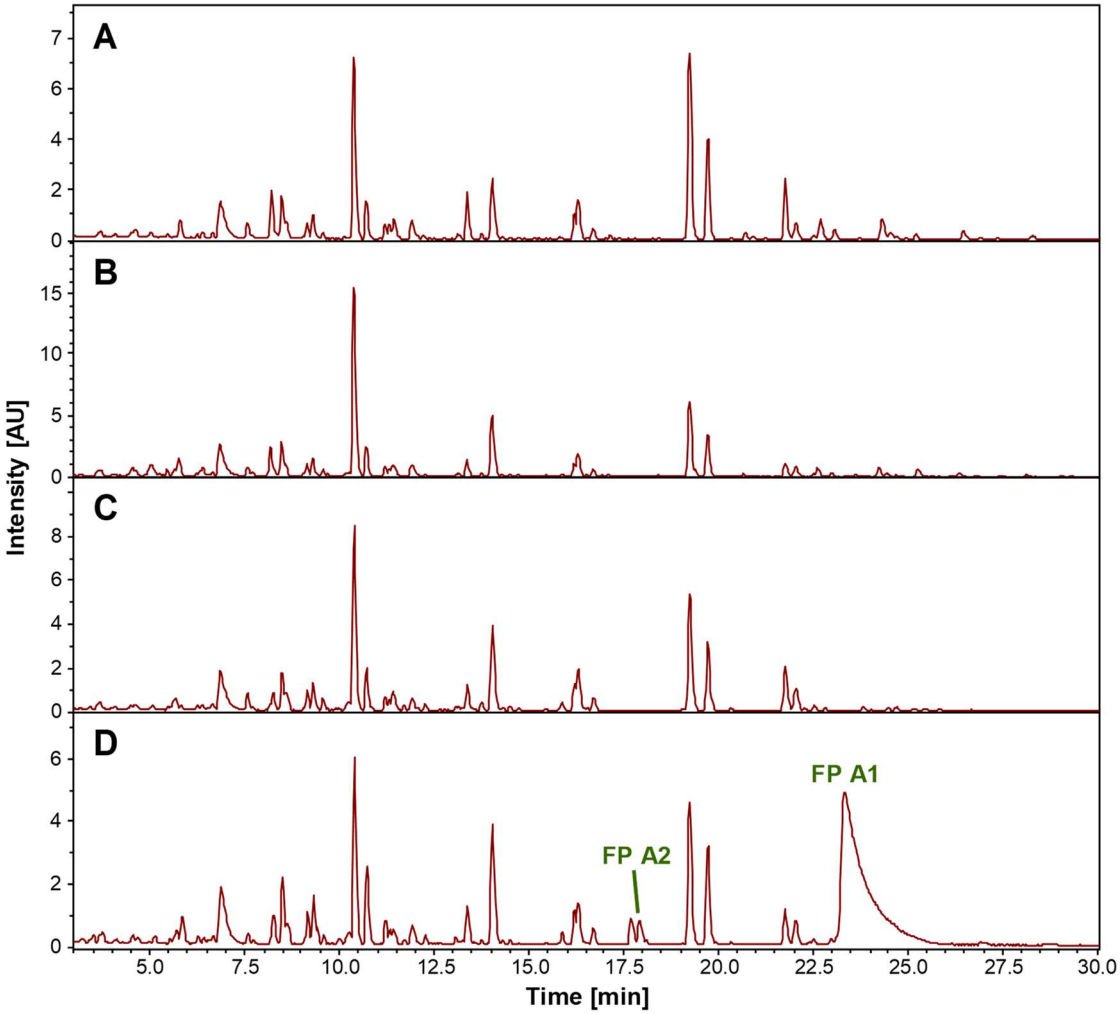

Figure S8. LC-HRESIMS spectra of heterologously expressed felipeptin A2 (A) and felipeptin A1 (B) showing the multiply protonated molecules.

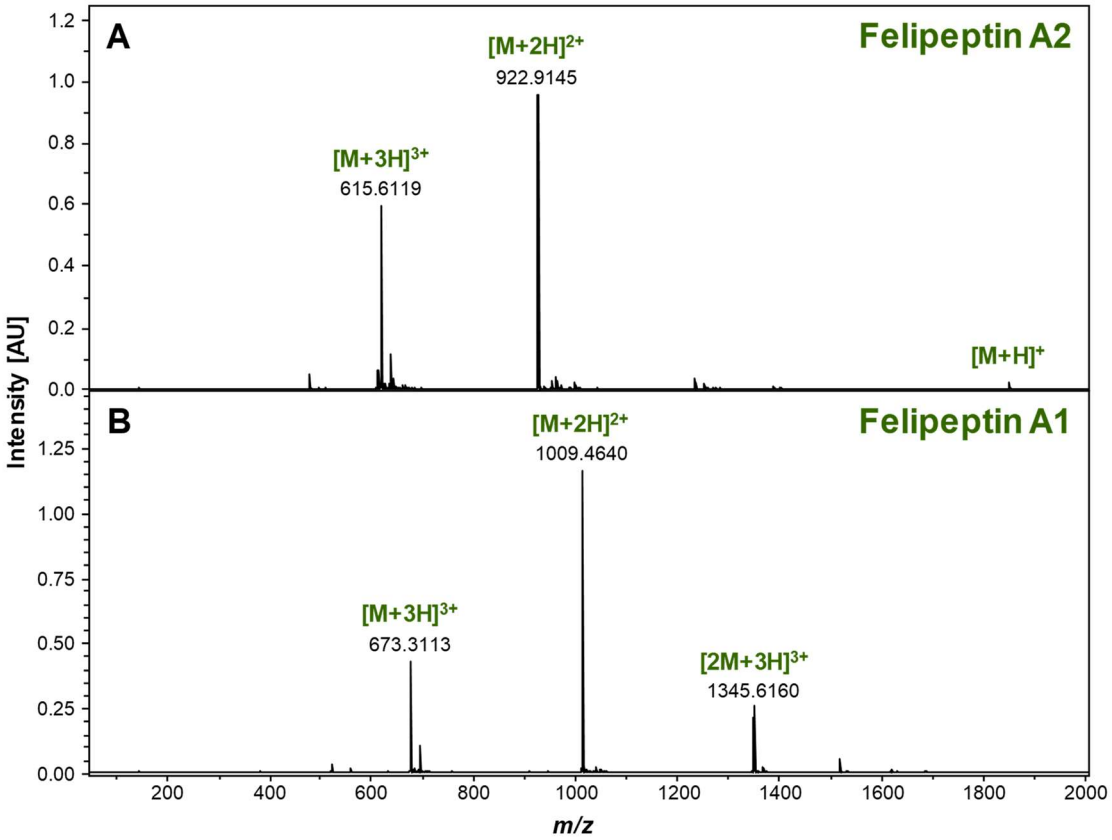

Figure S9. LC-MS analysis of purified felipeptin A1 obtained by heterologous production, Related to Figure 3. Positive ion mode base peak chromatogram in the range of *m/z* 150-2000 (A) and extracted ion chromatogram of *m/z* 1009.4616±0.0101 (B) of the purified felipeptin A1 (FP A1). A derivative carrying a methyl group on the C-terminal half of the peptide, which is presumably formed by C-terminal methylation during extraction with methanol, and a formylated derivative are observed as impurities.

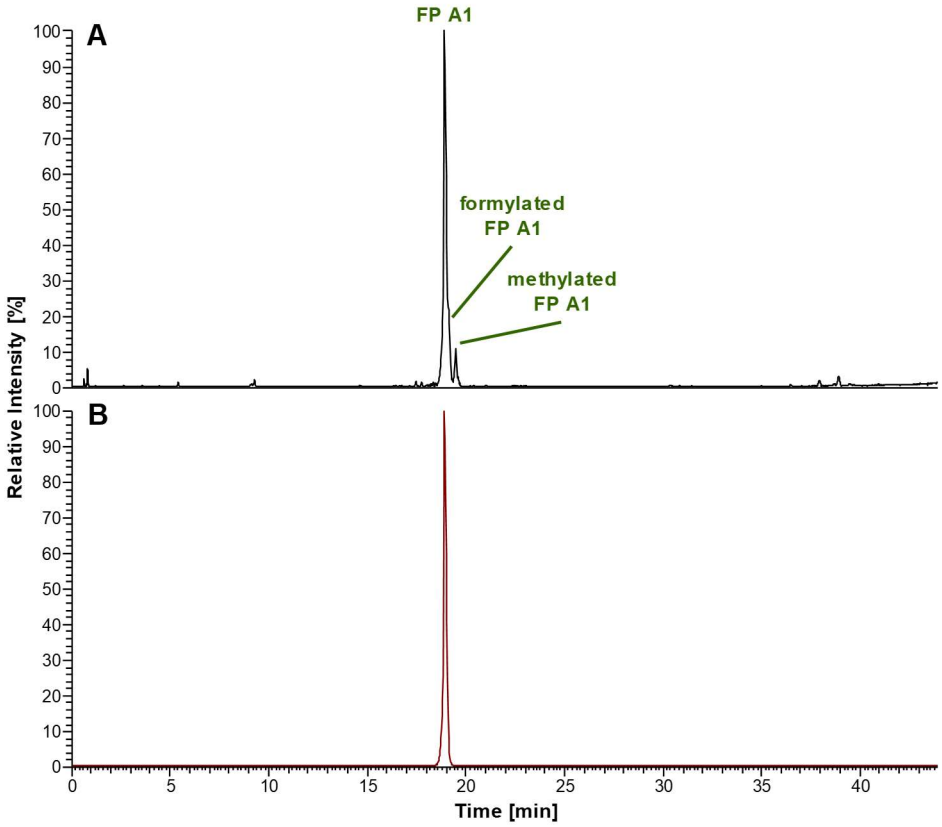

Figure S10. LC-MS analysis of purified felipeptin A2 obtained by heterologous production, Related to Figure 3. Positive ion mode base peak chromatogram in the range of *m/z* 50-2000 (A), extracted ion chromatogram of *m/z* 922.9140±0.0200 (B), and UV chromatogram at 190 nm (C) of the purified felipeptin A2.

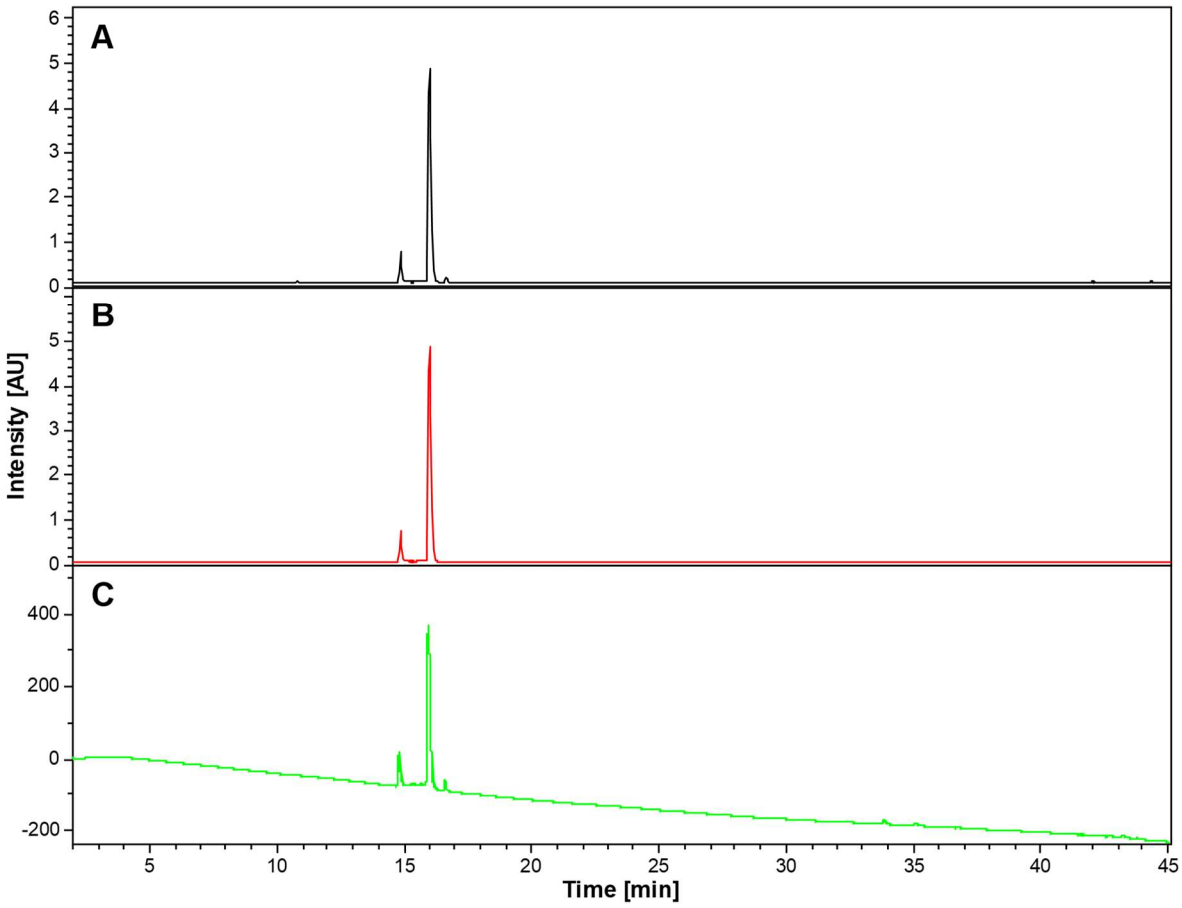

Figure S11. Bioassay against of felipeptin A1 (FA1), felipeptin A2 (FA2), mixture 1:1 (FA1/FA2) against *Bacillus subtilis*. Blanks; MeoH, MeOH + formic acid 6%.

Compound	Amoun (µg)
felipeptin A1 (FA1)	100
felipeptin A2 (FA2)	100
mixture 1:1 FA1/FA2	50/50

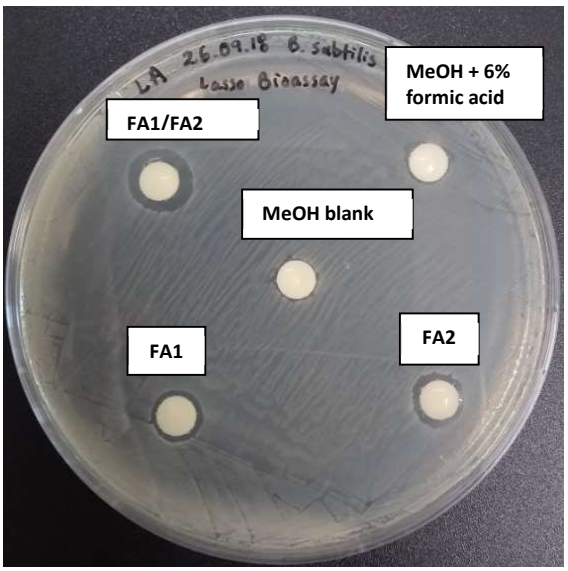

Figure S12. Effects of felipeptins' combinations in different cancer cell lines.(A-C) The relative cell survival of HCT116 (A), A375 (B), and normal BJ-fibroblast (C) cell lines upon combinational treatments with felipeptins A1 and A2, Related to Figure 5. Data shown are Mean ± SD, obtained in 3 independent experiments. * $p<0.05$, ** $0.01\leq p$ and *** $p<0.001$. (D-E) p53 deletion does not affect the synergistic induction of cell growth by felipeptins. Heatmaps on the left show changes of cell growth rate upon 72h treatment with different doses of felipeptins at a 2-fold serial dilution (as indicated in the figures) in cancer cell lines carrying p53 deletion MCF7p53KO (D) and A375p53KO (E), measured using rezasurin assay and normalized to DMSO control. Red indicates increased cell number, white – no change, blue – decreased cell number. Heatmaps on the right show HSA synergy score, indicated by green color (D-E). Data presented as mean log2 from two independent experiments performed in

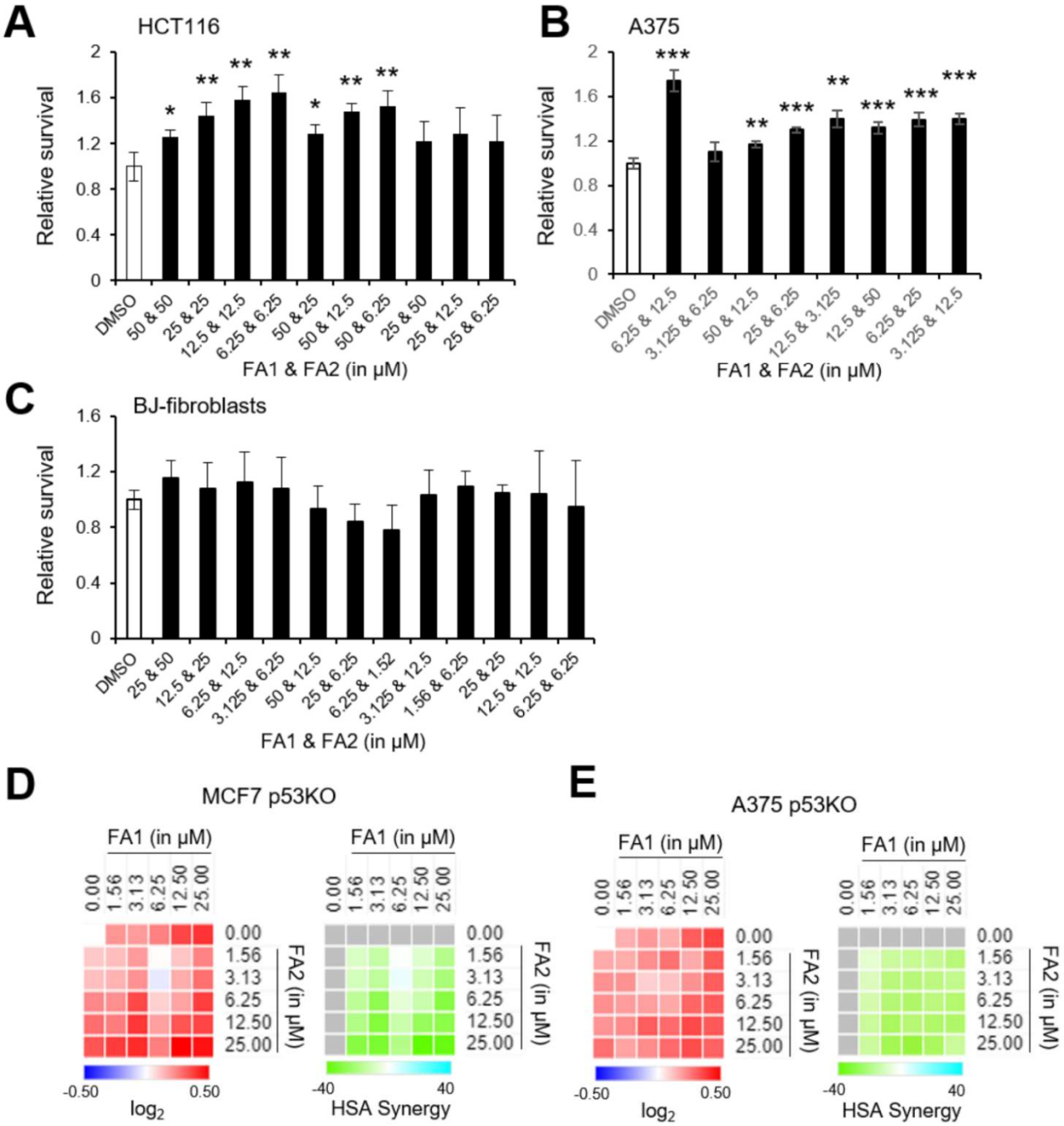

duplicate.

Figure S13. Interaction between felipeptins A1 and A2 in DMSO, Related to Figure 2. (A) Model of the interaction between felipeptin A1 (cyan) and A2 (orange), produced by HADDOCK (van Zundert et al., 2016). Residues of interest are labelled and their side-chains are shown. While this model illustrates one possible conformation of the A1:A2 complex, which is in agreement with NMR data, other conformations and interaction ratios (e.g. 1:2) cannot be ruled out.(B) Chemical shift perturbations in felipeptin A2 upon titration with felipeptin A1 (black); error bars represent a chemical shift error of 0.003 ppm. These chemical shift changes were fitted using a two-state model (red) (Krishnamoorthy et al., 2010) to obtain a K_d = 0.3 ± 0.2 mM. Since this interaction study was performed without isotopically enriching the peptides, i.e. with 1.1% natural-abundance ^{13}C, the sensitivity of the ^{13}C-HSQC spectra was remarkably low. This, combined with the viscosity of DMSO, resulted in broad peak shapes that complicated precise analysis of chemical shift perturbations. The high uncertainty in the K_d reflects these difficulties. However, a dissociation constant in the µM-mM range, like the estimate in this study, is characteristic of weak transient interactions (Perkins et al., 2010). (C) ^{15}N-HSQC spectra of A1 (green), A2 (red) and A1 mixed with A2 in a 1:1 ratio. Assigned H^N/N pairs are labeled. Chemical shift assignments of A1 and A2 have been deposited in the BMRB under the accession codes 34478 and 34479, respectively.

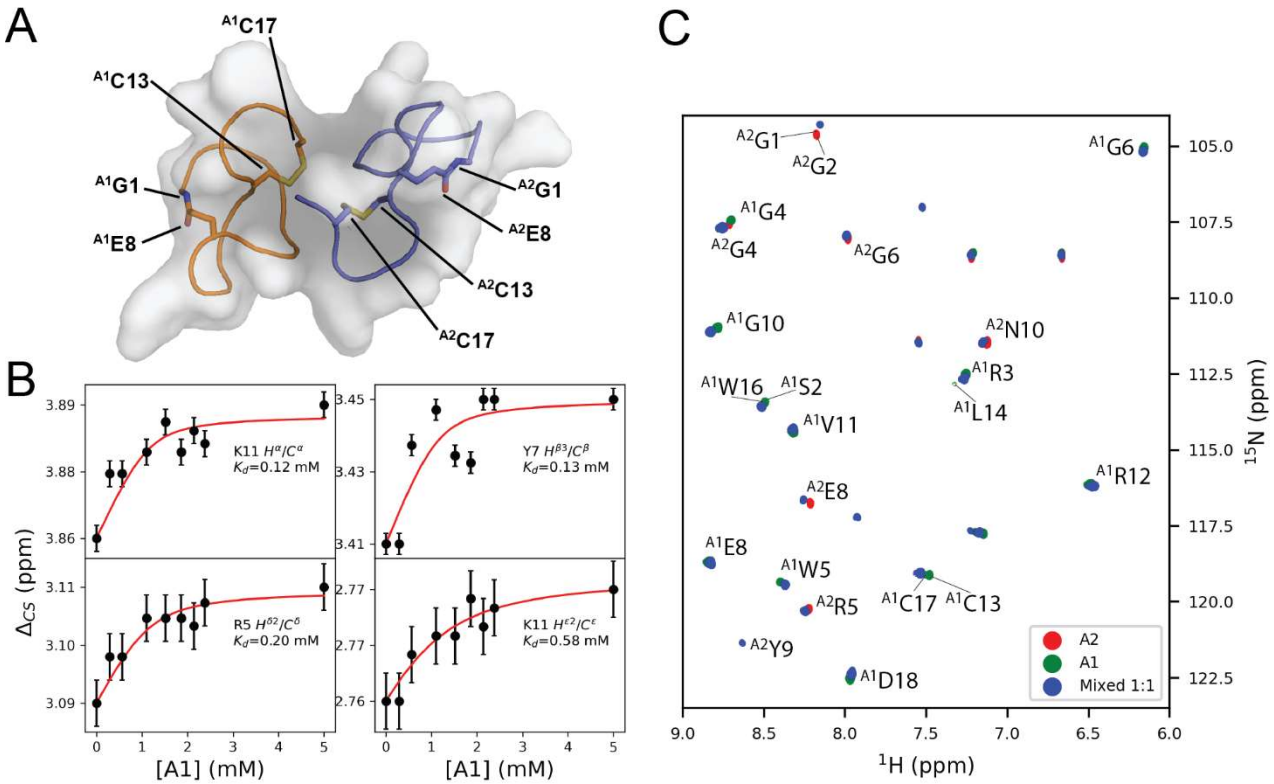

Figure S14. Thermal and proteolytic stability assay of purified felipeptin A1. Positive ion mode base peak chromatograms in the range of *m/z* 400-2000 of the control sample in aqueous solution (A), the same sample incubated at 95°C for 20h in the absence of the reducing agent dithiothreitol (DTT) (B), the sample incubated at 95°C for 20h in the presence of the reducing agent DTT (C), the sample incubated in 50 mM sodium acetate at room temperature for 20h in the presence of carboxypeptidase B (D), and the sample incubated in 50 mM sodium acetate at room temperature for 20h in the presence of carboxypeptidase Y (E). Felipeptin A1 (**1**, *m/z* 1009.4642, $[M+2H]^{2+}$, *G*SRGWGF*E*PGVR*C*LIW*C*D) showed no sign of thermal unthreading after 20h at 95°C, even though partial hydrolytic cleavage of the C-terminal Asp18 was already observed (**3**, *m/z* 951.9503, $[M+2H]^{2+}$, *G*SRGWGF*E*PGVR*C*LIW*C*). In addition, the formylated derivative (**2**, *m/z* 1023.4619, $[M+2H]^{2+}$) is completely hydrolyzed presumably to yield unmodified felipeptin A1 under these conditions. After incubation at 95°C for 20h in the presence of the reducing agent DTT not only the reduced versions of felipeptin A1 (**4**, *m/z* 1010.4718, $[M+2H]^{2+}$, *G*SRGWGF*E*PGVRCLIWCD and the truncated felipeptin A1 (**5**, *m/z* 952.9579, $[M+2H]^{2+}$,*G*SRGWGF*E*PGVRCLIWC) were detected, but also numerous degradation products such as a prominent product cleaved after Arg12 (**6**, *m/z* 643.8243, $[M+2H]^{2+}$, *G*SRGWGF*E*PGVR). Felipeptin A1 was stable towards carboxypeptidases B and Y under the test conditions.

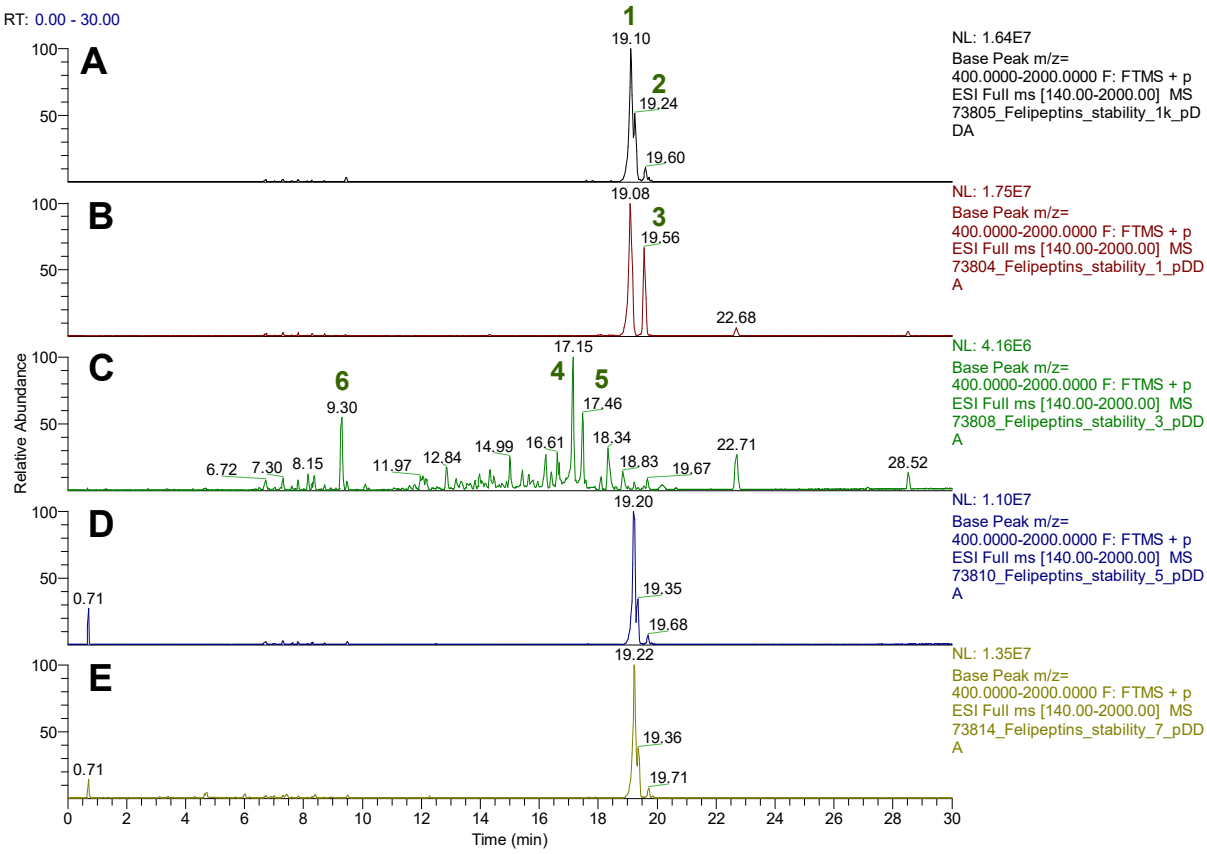

Figure S15. Thermal and proteolytic stability assay of purified felipeptin A2. Positive ion mode base peak chromatograms in the range of *m/z* 400-2000 of the control sample in aqueous solution (A), the same sample incubated at 95°C for 20h in the absence of the reducing agent DTT (B), the sample incubated at 95°C for 20h in the presence of the reducing agent DTT (C), the sample incubated in 50 mM sodium acetate at room temperature for 20h in the presence of carboxypeptidase B (D), and the sample incubated in 50 mM sodium acetate at room temperature for 20h in the presence of carboxypeptidase Y (E). Felipeptin A2 (**1**, *m/z* 922.9160, $[M+2H]^{2+}$, *G*GGGRGY*E*YNKQ*C*LIF*C*) gives a second, minor peak (**2**, *m/z* 922.9156, $[M+2H]^{2+}$, *G*GGGRGY*E*YNKQ*C*LIF*C*) in the chromatogram with identical mass and MS/MS spectrum. This could be an alternative stable conformation as in the case of the lasso peptide benenodin-1(Zong et al., 2017), but further experiments are required to elucidate the structural difference of the minor species. While the abundance of this species is not significantly changed after 20h at 95°C, a third peak of an isobaric species is observed which is interpreted as unthreaded branched-cyclic felipeptin A2 (**3**, *m/z* 922.9162, $[M+2H]^{2+}$, *G*GGGRGY*E*YNKQ*C*LIF*C*). After incubation at 95°C for 20h in the presence of the reducing agent DTT not only the reduced versions of felipeptin A2 (**4**, *m/z* 923.9247, $[M+2H]^{2+}$, *G*GGGRGY*E*YNKQCLIFC was detected, but also numerous degradation products such as a prominent truncated product cleaved after Phe16 (**5**, *m/z* 872.4197, $[M+2H]^{2+}$, *G*GGGRGY*E*YNKQCLIF). Felipeptin A2 was stable towards carboxypeptidases B and Y under the test conditions.

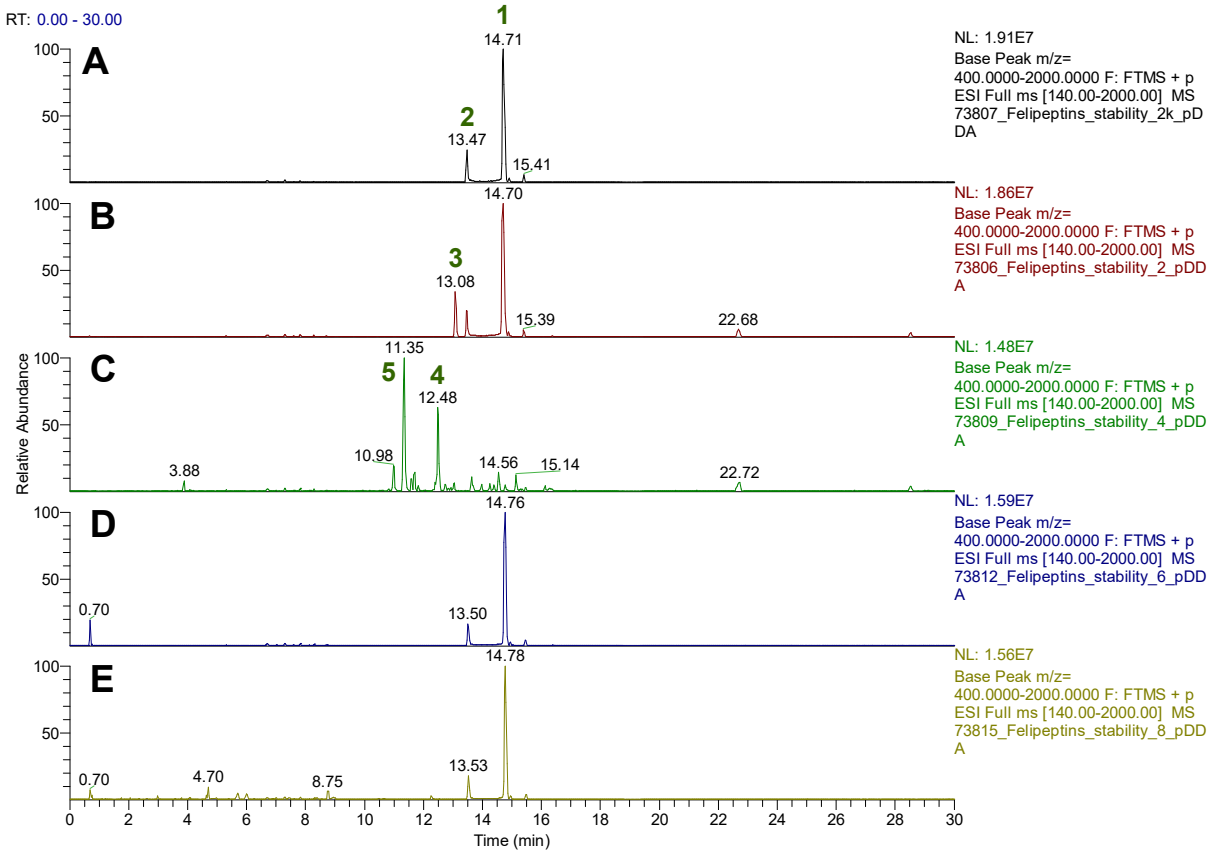

Figure S16. Thermal and proteolytic stability assay of purified felipeptin A2. LC-HRESIMS/MS spectra of the $[M+2H]^{2+}$ ion at *m/z* 922.916 of the three conformers of felipeptin A2 observed after incubation at 95°C for 20h in the absence of the reducing agent DTT (see Fig. S14). The MS/MS spectrum of the main peak (**1**), representing the native lasso-fold as confirmed by NMR experiments, (A) is undistinguishable from the MS/MS spectrum of a minor presumed conformer (**2**) that is already present at room temperature (B). The presumed unthreaded branched-cyclic felipeptin A2 (**3**) shows identical fragment ions but a clear shift in relative intensities.

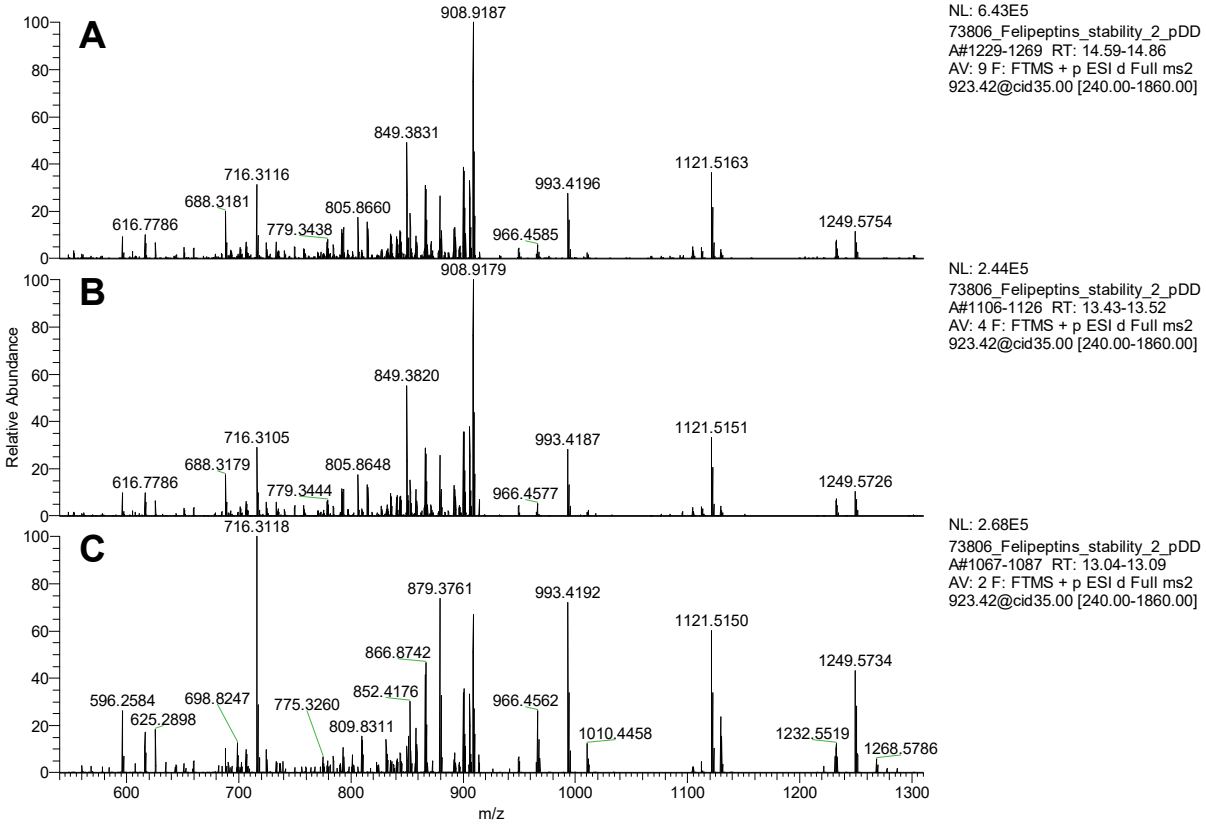

Figure S17. Evidence for the lasso topology in the MS/MS spectrum of felipeptin A1, related to Figure 2. LC-HRESIMS/MS spectra of the $[M+3H]^{3+}$ ion at *m/z* 673.3116 of felipeptin A1 (**1**) in the sample incubated at 95°C for 20h in the absence of the reducing agent DTT (A), and the of the $[M+3H]^{3+}$ ion at *m/z* 673.9839 of reduced felipeptin A1 (**4**) in the sample incubated at 95°C for 20h in the presence of the reducing agent DTT (B).

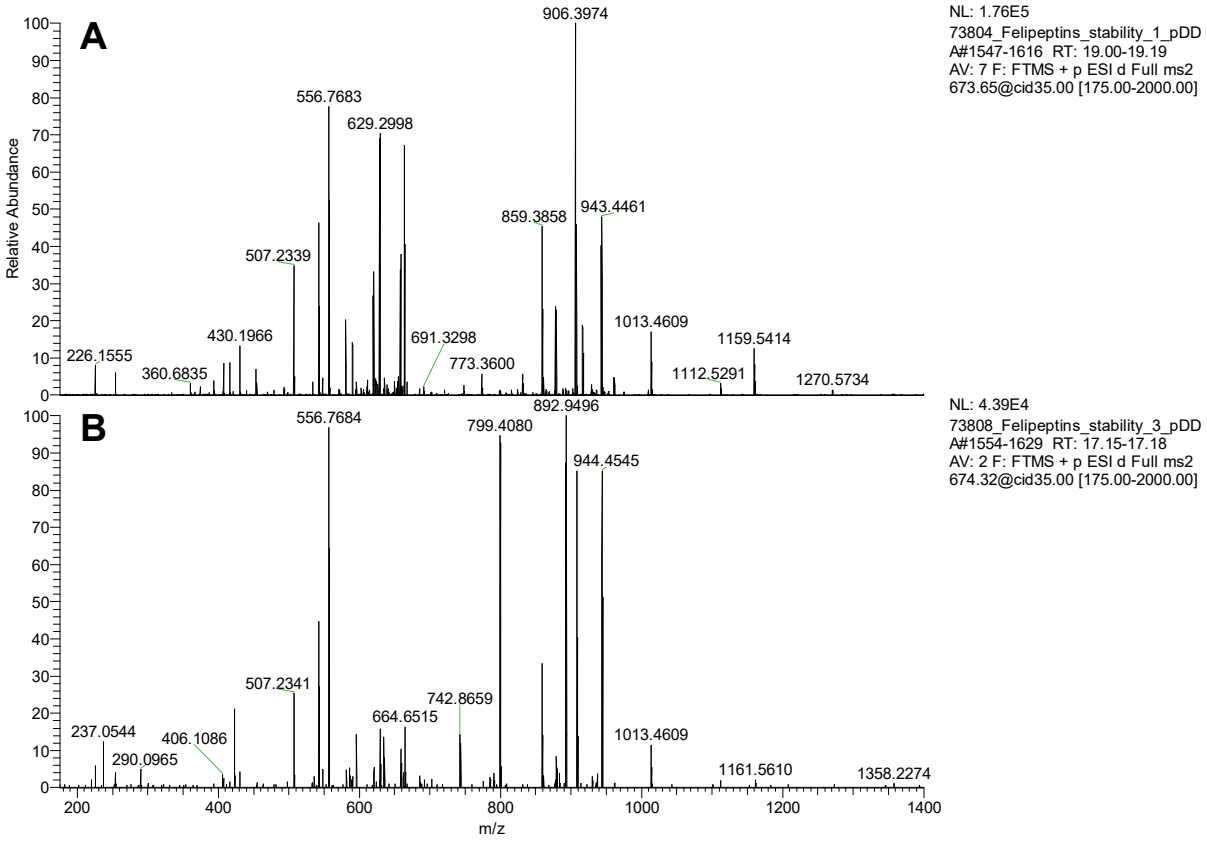

Figure S18. Evidence for the lasso topology in the MS/MS spectrum of felipeptin A1, Related to Figure 2. Zoom into the LC-HRESIMS/MS spectra of the $[M+3H]^{3+}$ ion at *m/z* 673.3116 of felipeptin A1 (**1**) in the sample incubated at 95°C for 20h in the absence of the reducing agent DTT (A), and the of the $[M+3H]^{3+}$ ion at *m/z* 673.9839 of reduced felipeptin A1 (**4**) in the sample incubated at 95°C for 20h in the presence of the reducing agent DTT (B). The fragment ion at *m/z* 960.9377 labelled $[(b_8)^*(y_9)]^{2+}$ originates from the loss of Pro9 from the loop region and represents a noncovalently interlocked fragment that is an additional strong evidence for the lasso topology (Jeanne Dit Fouque et al., 2018)

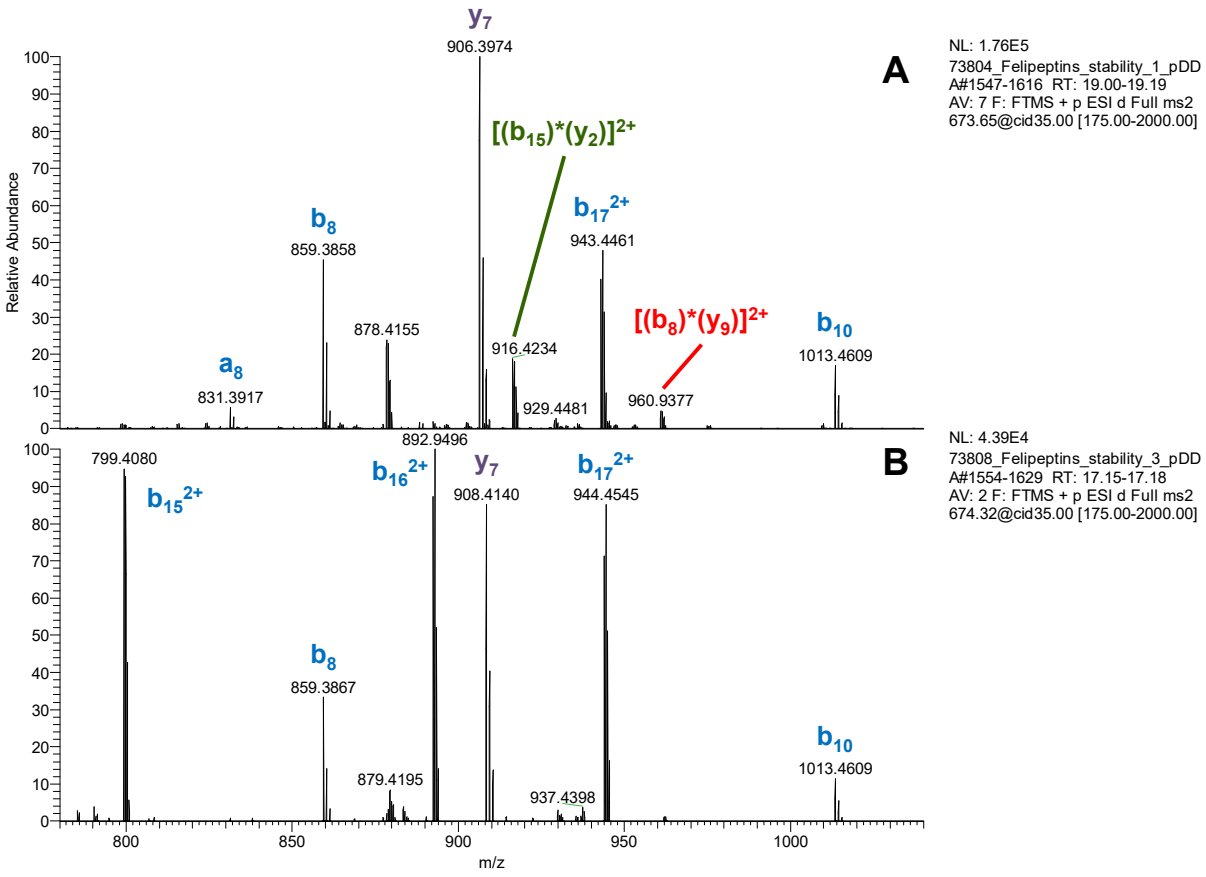

Supplemental Tables

Table S1. Bacterial strains and vectors used in this work.

Strain	**Function**	**Genotype/phenotype**
Escherichia coli DH5α	General cloning host	luxS supE44 ΔlacU169 (ϕ80 lacZΔM15) hsdR17, recA1, endA1, gyrA96, thi-1, relA1
E. coli ET12567 (pUZ8002)	Non-methylating strain with pUZ8002 helper plasmid and RP4 oriT for conjugation	dam− , dcm− , hsdM−, KanR, CmlR
E. coli BW25113/pKD46	λ RED recombination system (pKD46)	rrnB3, ΔlacZ4787, hsdR514, Δ(araBAD)567, Δ(rhaBAD)568 rph-1, repA101(ts), araBp-gam-bet-exo, oriR101, AmpR
E. coli EPI300-T1	Genome library construction and overproduction of fosmids.	F– mcrA Δ(mrr-hsdRMS-mcrBC) (StrR), φ80dlacZΔM15, ΔlacX74, recA1, endA1, araD139 Δ(ara, leu)7697, galU, galK, λ– rpsL nupG, trfA, tonA, dhfr
Streptomyces coelicolor M1154	Host for heterologous expression	Δact Δred Δcpk Δcda rpoB[C1298T] rpsL[A262G]
Streptomyces albus J1074	Host for heterologous expression	Wild type
Vector	**Function**	**Characteristics**
pCC1FOS (Epicentre)	Genome library construction. Fosmid used for heterologous expression.	8.1 kb, ClmR, lacZ, loxP, cos, parC, parB, parA, repE, ori2, oriV, redF
pSOK806	Integrative plasmid with strong ermE promoter.	5.7 kb, ermE*p, ColEI oriR, AmR, , $oriT^{RP4}$, int-$attP^{VWB}$
pSET152	Integrative plasmid. Use as a control for heterologous expression.	5.5 kb, lacZα ori^{pUC19}, $oriT^{RP4}$, int-$attP^{\varphi C31}$, aac(3)IV

Table S2. List of oligonucleotide primers used in this work.

Oligo name	Sequence (5´-3´)	Characteristics
pCC1FOS-FP	GGATGTGCTGCAAGGCGATTAAGTTGG	pCC1FOS forward sequencing primer
pCC1FOS-RP	CTCGTATGTTGTGTGGAATTGTGAGC	pCC1FOS reverse sequencing primer
Fw_Cluster21_A	TTGGTGCGCTGGATGTC	Lasso peptide cluster screening part A forward sequencing primer
Rv_Cluster21_A	TCTGTGGTGGCTGATTC	Lasso peptide cluster screening part A reverse sequencing primer
Fw_Cluster21_B	AGTACCGCCGCGTATTC	Lasso peptide cluster screening part B forward sequencing primer
Rv_Cluster21_B	AGCTACCGCCTGAAGTG	Lasso peptide cluster screening part B reverse sequencing primer
Fw_Cluster21_C	GGCGGATCAGGTAGATG	Lasso peptide cluster screening part C forward sequencing primer
Rv_Cluster21_C	ACGTCAGCGAAGCCATC	Lasso peptide cluster screening part C reverse sequencing primer
SARP_Fw	GTCA*GAATTC*GTGGCAATCGCGTTGCAC	SARP regulator forward sequencing primer (EcoRI restriction site)
SARP_Rv	GTCA*GATATC*GCGACGTACGACGACGAATC	SARP regulator reverse sequencing primer (EcoRV restriction site)

Table S3. Some features of the *Amycolatopsis* sp. YIM10 genome.

Genome Feature	Chromosome
Genome size (bp)	10,312,959
No. of scaffolds	1
No. of genes	9,732
No. of t(m)RNA genes	112
G+C mol %	71.25

Table S4.
BGCs identified in the genome of *Amycolatopsis* sp. YIM10 with antiSMASH 5.0 and manually curated to resolve ambiguous cluster borders, Related to Figure 1. BGCs which homologs could not be identified in other bacterial genomes are shaded in grey.

No	Cluster type	Putative product	Presence in another bacterium
1	Ectoine	ectoine	*Amycolatopsis albispora* WP1
2	PKSI	glycosylated polyketide	-
3	Terpene	carotenoid	*Amycolatopsis albispora WP1*
4	Terpene	brasilicardin-like terpenoid	*Saccharopolyspora erythraea* NRRL2338
5	Other	halogenated NR peptide	*Amycolatopsis nigrescens* CSC17Ta-90
6	Bacteriocin	bacteriocin	-
7	Terpene	lipoprotein-terpenoid	*Amycolatopsis albispora* WP1
8	PKSI-NRPS	glycosylated PKSI-NRPS	*Amycolatopsis albispora* WP1
9	NRPS	NR peptide	*Amycolatopsis albispora* WP1
10	Terpene	carotenoid	*Amycolatopsis albispora WP1*
11	NRPS	NR peptide	-
12	PKSIII	1,2,4-trimethoxynaphthalene?	*Amycolatopsis albispora WP1*
13	Oligosaccharide-NRPS	halogenated-glycosylated NR peptide	-
14	PKSI-NRPS	PK-NR peptide hybrid	-
15	NRPS	anthramycin	*Nocardia brasiliensis* NBRC 14402
16	PKSI-NRPS	PK-NR peptide hybrid	-
17	Ladderane-NRPS	carbamoylated ladderane-NR peptide	-
18	NRPS	mirubactin	*Amycolatopsis albispora WP1*
19	Arylpolyene-Ladderane	halogenated arylpolyene-ladderane	-
20	NRPS	halogenated NR peptide	-
21	**Lasso peptide**	**lasso peptide**	**-**
22	PKSI	macrolide	*Streptomyces iranensis* DSM 41954
23	Phosphonate	phosphonate	*Amycolatopsis cihanbeyliensis* DSM 45679
24	Betalactone	betalactone	*Amycolatopsis albispora WP1*
25	Indole	indole	*Amycolatopsis albispora WP1*
26	Siderophore	siderophore	*Amycolatopsis albispora WP1*
27	Bacteriocin	bacteriocin	*Amycolatopsis albispora WP1*
28	NRPS	NR peptide	*Amycolatopsis albispora WP1*
29	PKSI	glycosylated polyketide	*Amycolatopsis albispora WP1*
30	NRPS	citrullin-containing NR peptide	-
31	NRPS	glycosylated NR peptide	*Amycolatopsis thermoflava N1165*
32	PKSI	polyketide	*Kibdelosporangium aridum DSM 44150*
33	Other	unknown	-
34	Betalactone	betalactone	*Amycolatopsis albispora WP1*
35	NRPS	cephamycin C	*Amycolatopsis lactamdurans*
36	PKS-NRPS	PK-NR peptide hybrid	*Amycolatopsis albispora WP1*
37	PKSI	glycosylated polyene macrolide	*Amycolatopsis albispora WP1*
38	Terpene	terpenoid	*Amycolatopsis albispora WP1*
39	NRPS	albachelin	*Amycolatopsis albispora WP1*
40	PKSI	quartromicin	*Amycolatopsis albispora WP1*
41	Lantipeptide	lantipeptide	*Amycolatopsis albispora WP1*
42	PKSI-NRPS	PK-NR peptide hybrid	*Amycolatopsis albispora WP1*
43	LAP	lingual antimicrobial peptide	*Amycolatopsis albispora WP1*
42	PKSI	glycosylated polyketide	*Amycolatopsis albispora WP1*
43	Lantipeptide	lantibiotic, class III	*Amycolatopsis* sp. 8-3EHSu
44	Butyrolactone-PKSI	unknown	*Amycolatopsis albispora WP1*

Table S5. Minimal inhibitory concentrations (MIC) (μg/mL) of felipeptin A1 (FA1), felipeptin A2 (FA2) and their 1:1 mixture against *Streptococcus pyogenes* and *Streptococcus pneumoniae* ATCC 49619. Controls: daptomycin, erythromycin and vancomycin.

Compound	**MIC: *Streptococcus pyogenes* (μg/mL)**	**MIC: *Streptococcus pneumoniae* (μg/mL)**
Felipeptin A1	>128	64
Felipeptin A2	>128	>128
Felipeptins A1+A2	64	64
Daptomycin	8	32
Erythromycin	<1	<1
Vancomycin	<1	<1

References

Bredholdt, H., Galatenko, O.A., Engelhardt, K., Fjaervik, E., Terekhova, L.P., and Zotchev, S.B. (2007) Rare actinomycete bacteria from the shallow water sediments of the Trondheim fjord, Norway: isolation, diversity and biological activity. Environ. Microbiol. *9*, 2756-2764.

Calcagno, A.M., Salcido, C.D., Gillet, J.P., Wu, C.P., Fostel, J.M., Mumau, M.D., Gottesman, M.M., Varticovski, L., and Ambudkar, S.V. (2010) Prolonged Drug Selection of Breast Cancer Cells and Enrichment of Cancer Stem Cell Characteristics. J. Natl. Cancer Inst. *102*, 1637-1652.

Di Veroli GY, Fornari C, Wang D, Mollard S, Bramhall JL, Richards FM, Jodrell DI. (2016) Combenefit: An Interactive Platform for the Analysis and Visualization of Drug Combinations. Bioinformatics *32*, 2866-2868.

Flett, F., Mersinias, V., and Smith, C.P. (1997) High efficiency intergeneric conjugal transfer of plasmid DNA from Escherichia coli to methyl DNA-restricting streptomycetes. FEMS Microbiol. Lett. *155*, 223-229.

Gordon, D., and Green, P. (2013) Consed: a graphical editor for next-generation sequencing. Bioinformatics *29*, 2936-2937.

Güntert, P. (2004) Automated NMR structure calculation with CYANA Methods Mol. Biol. *278*, 353–378.

Gust, B. (2009) Chapter 7. Cloning and analysis of natural product pathways. Methods Enzymol. *458*, 159-180.

Israel, D.I. (2006) PCR-Based Screening of DNA Libraries. CSH Protoc. *2006(1)*, pdb.prot4129.

Jeanne Dit Fouque, K., Bisram, V., Hegemann, J.D., Zirah, S., Rebuffat, S., and Fernandez-Lima, F. (2019). Structural signatures of the class III lasso peptide BI-32169 and the branched-cyclic topoisomers using trapped ion mobility spectrometry-mass spectrometry and tandem mass spectrometry. Anal. Bioanal. Chem. *411*, 6287-6296.

Keller, R. (2004) The Computer Aided Resonance Assignment Tutorial, CANTINA Verlag, Goldau, Switzerland.

Krishnamoorthy, J., Yu, V.C., and Mok, Y.K. (2010) Auto-FACE: an NMR based binding site mapping program for fast chemical exchange protein-ligand systems. PLoS ONE *5*, e8943.

Perkins, J.R., Diboun, I., Dessailly, B.H., Lees, J.G., and Orengo, C. (2010) Transient protein-protein interactions: structural, functional, and network properties. Structure *18*, 1233-1243.

Peuget, S., Zhu, J., Sanz, G., Singh, M., Gaetani, M., Chen, X., Shi, Y., Saei, A.A., Visnes, T., Lindström, M.S. et al. (2020) Thermal Proteome Profiling Identifies Oxidative-Dependent Inhibition of the Transcription of Major Oncogenes as a New Therapeutic Mechanism for Select Anticancer Compounds. Cancer Res. *80*, 1538-1550.

Seemann, T. (2014) Prokka: Rapid Prokaryotic Genome Annotation. Bioinformatics *30*, 2068-2069.

Sekurova, O.N., Zhang, J., Kristiansen, K.A., and Zotchev, S.B. (2016) Activation of Chloramphenicol Biosynthesis in *Streptomyces venezuelae* ATCC 10712 by Ethanol Shock: Insights From the Promoter Fusion Studies. Microb. Cell Fact. *15*, 85.

van Zundert, G.C.P., Rodrigues, J.P.G.L.M., Trellet, M., Schmitz, C., Kastritis, P.L., Karaca, E., Melquiond, A.S.J., van Dijk, M., de Vries, S.J., and Bonvin, A.M.J.J. (2016) The HADDOCK2.2 Web Server: User-Friendly Integrative Modeling of Biomolecular Complexes. J. Mol. Biol. *428*, 720-725.

Zong, C., Wu, M.J., Qin, J.Z., and Link, A.J. (2017). Lasso Peptide Benenodin-1 Is a Thermally Actuated [1]Rotaxane Switch. J. Am. Chem. Soc. *139*, 10403-10409.